Physics – Uspekhi **49** (7) 693 – 718 (2006)

REVIEWS OF TOPICAL PROBLEMS PACS numbers: **61.10. – i**, **61.12. – q**, 61.66.Fn, 61.72.Ji

Short-range order and diffuse scattering in nonstoichiometric compounds

A I Gusev

DOI: 10.1070/PU2006v049n07ABEH005972

Contents

Abstract. Diffraction studies of nonstoichiometric compounds have revealed various diffusion scattering effects caused by formation of a short-range order related to substitutions of atoms and vacancies (or different-sort atoms) or to atomic displacements. For nonstoichiometric compounds, we consider experimental results on short-range order that are obtained from diffuse neutron and X-ray scattering and electron diffraction. The occurrence of diffuse intensity maxima in diffraction patterns is shown to result from a redistribution of nonmetallic atoms and structural vacancies in disordered nonstoichiometric carbides, nitrides, and oxides or of mutually substitutable atoms in solid solutions of nonstoichiometric compounds at the stage preceding the formation of a long-range order. Applications of the transition-state cluster model for the description of the topology of the diffuse scattering intensity in nonstoichiometric compounds with the substitutional short-range order are discussed. Flat extended diffusive scattering regions obtained in diffraction patterns for ordered phases, not passing through structural sites of the reciprocal lattice, are shown to occur due to atomic displacement waves.

1. Introduction

Intense studies of oxides, sulfides, and selenides of transition metals performed in the 1940s – 1950s revealed the existence of nonstoichiometric phases with wide homogeneity regions. For example, according to various data, the cubic titanium monoxide TiO has the homogeneity region from $TiO_{0.65-0.80}$ to $TiO_{1.25-1.33}$. Later, it was shown that the widest homogeneity regions are characteristic of cubic carbides and nitrides MC_y and MN_y (or $MC_y\square_{1-y}$ and $MN_y\square_{1-y}$, where $\square$ is the structural vacancy and $0.5 \leqslant y \leqslant 1.0$) of transition metals of Groups IV and V. Wide homogeneity regions are also characteristic of ternary compounds related to carbides and nitrides, such as carbosilicides $M_5Si_3C_x$, siliconitrides $M_5Si_3N_x$, and silicoborides $M_5Si_3B_x$ with structures of the Cr_2AlC and $A13$ (β-Mn) types, and of complex oxides $L_{1-x-z}\square_yM_{1+x}O_2$ (where L is an alkali metal and M is a transition metal) such as lithium nickelate, in which the atoms of alkali and transition metals substitute one another and the metallic sublattice contains a large number of structural vacancies.

The above-mentioned and some other compounds form a group of strongly nonstoichiometric compounds [1, 2]. Their main feature is the high concentration of structural vacancies, which at the lower boundary of the homogeneity region can reach several dozen (atomic) percent. The principal features of the structure and properties of strongly nonstoichiometric compounds have been described in [1 – 5].

A specific feature of structural vacancies $\square$ as structure defects is that their concentration is directly related to chemical composition. In nonstoichiometric compounds, the structural vacancies are analogs of atoms, i.e., they behave as quasiparticles; in their sublattice, they play the same role as the atoms of this sublattice. In the majority of nonstoichiometric compounds, structural vacancies exist only in one of the sublattices. However, nonstoichiometric compounds are known that contain structural vacancies in two sublattices; depending on the compound composition, the concentration of vacancies in the sublattices can be equal or different. The simultaneous presence of structural vacancies in both metallic and nonmetallic sublattices is characteristic of titanium and

A I Gusev Institute of Chemistry, Ural Division,
Russian Academy of Sciences,
ul. Pervomaiskaya 91, Ekaterinburg 620219, Russian Federation
Tel. (7-343) 374 73 06. Fax (7-343) 374 44 95
E-mail: gusev@ihim.uran.ru

Received 17 November 2005
Uspekhi Fizicheskikh Nauk **176** (7) 717 – 743 (2006)
Translated by S N Gorin; edited by A M Semikhatov

vanadium cubic monoxides, niobium nitride, and some other nitrides.

The very high concentration of vacancies in strongly nonstoichiometric compounds led to the question of how the vacancies are distributed in the crystal lattice.

From the formal standpoint, the vacant sites of the crystal lattice of nonstoichiometric compounds behave as atoms that occupy sites of the same lattice. For this reason, the structural vacancies □ are considered a certain analog of atoms rather than merely 'holes' in the crystal lattice. The deviation from stoichiometry and the related homogeneity region can be regarded as a substitutional solid solution whose components are atoms and vacancies. Thus, in the structure of a nonstoichiometric compound, e.g., MX_y ($MX_y\square_{1-y}$), the atoms X and vacancies □ form a substitutional solution, which can be either disordered or ordered. The concept of a vacant site as a structural element of crystals analogous to an occupied site emerged in the 1960s – 1970s, when problems of nonstoichiometry and ordering in oxides, sulfides, and chalcogenides were actively discussed in the literature.

In substitutional solid solutions, the symmetry of a crystal lattice is retained even in the presence of disorder. Indeed, a substitutional solid solution is disordered at a sufficiently high temperature, and it is therefore impossible to indicate which sort of atom occupies a given site **r**. But the probability of occupation of this site by an atom of a given sort is known; this probability coincides with the concentration of these atoms. In nonstoichiometric compounds, the substitutional solution is formed by atoms and structural vacancies □ that are in the same sublattice. For example, in the nonstoichiometric compound $MX_y\square_{1-y}$, the probability of occupation of a site of the nonmetallic sublattice with an atom X is equal to y and the probability that this site is not occupied with an atom, i.e., is vacant, is $1 - y$. In other words, there is a certain lattice of probabilities that has all the properties of a crystal symmetry. As the temperature decreases, a redistribution of atoms and vacancies over the lattice sites can occur; as a result, some lattice sites become predominantly occupied with atoms X, whereas other sites are vacant. Thus, two opposite tendencies can be distinguished in the structure of nonstoichiometric compounds: the tendencies to ordering and to disordering. An ordered vacancy distribution is most probable at low temperatures; a disordered distribution exists at high temperatures, when the entropy contribution to the free energy of a nonstoichiometric compound is sufficiently large. The completely ordered and completely disordered distributions are the limit states of a nonstoichiometric compound. As a result of ordering, one or several ordered phases arise in the homogeneity region of the nonstoichiometric compound, which can also have their homogeneity regions. The maximum degree of long-range order, equal to unity, is reached for ordered phases that have a stoichiometric composition. Intermediate states, including a short-range order, exist between a chaotic (disordered, random) distribution of structural vacancies and the long-range order in their distribution.

Thus, the existence of nonstoichiometry is a prerequisite for either a disorder or order in the distribution of atoms and vacancies in the structure of nonstoichiometric compounds.

Deviations from a statistical (disordered) distribution of atoms and vacancies is primarily reflected in the crystal structure of nonstoichiometric compounds in the appearance of a short-range order or long-range order.

A short-range order is a state in which atoms of a given sort are preferentially surrounded with atoms of the same or a different sort in a disordered solid solution, i.e., a deviation from a statistical distribution of atoms over the crystal lattice sites occurs. In diffraction patterns, the presence of a short-range order manifests itself in the appearance of three-dimensional regions of diffuse scattering in reciprocal space. Along with a 'substitutional short-range order,' a 'displacement short-range order' can exist, related to static and dynamic displacements of atoms from positions corresponding to a certain 'mean' lattice. Static displacements, which arise in crystals with a substitutional disorder because of the differences in the sizes of atoms of different sorts, additionally modulate diffuse scattering. Thermal vibrations, i.e., dynamic displacements, lead to the appearance of a component of diffuse scattering such as the thermal Debye scattering.

Short-range order characterizes only the radial distribution of atoms, i.e., fluctuations of atomic concentrations in various coordination shells. Long-range order also includes an angular distribution and therefore allows determining which kind of atom resides in this or that lattice site. Taking the short-range order into account is especially important in those cases where no long-range order exists but correlations in the mutual position of atoms are present. The presence of correlations is a consequence of the difference in the energies of interaction of atoms of the same and of different sorts.

Long-range order and related effects of ordering on the structure and properties of nonstoichiometric compounds have been studied in sufficient detail (see, e.g., [1 – 5]). Short-range order has been studied much less, because the related effects are pronounced much more weakly.

The main experimental methods for studying short-range order in strongly nonstoichiometric compounds are nuclear magnetic resonance (NMR), diffuse scattering of neutrons or electrons (in studying the distribution of interstitial atoms), X-ray diffuse scattering (in studying the distribution of metallic atoms), and measurements of magnetic susceptibility. The specific features and results of the application of NMR and measurements of magnetic susceptibility for the investigation of short-range order in nonstoichiometric compounds have been discussed in much detail in several reviews [6 – 9]. As regards the investigations of short-range order in nonstoichiometric compounds by the methods of diffuse scattering, these results and their interpretation have been presented to date only in original works and have not been considered in a generalized form. In this work, we attempt to fill this gap and to attract the attention of experimentalists to interesting structural subjects such as nonstoichiometric compounds.

2. Short-range order parameters

In the absence of long-range order, the structural state of a solid solution, i.e., the character of the relative position of atoms of different sorts over crystal lattice sites, can be described using specific short-range order parameters.

There exist several variants for defining the short-range order parameter α and the correlation parameter $\varepsilon(R_i)$ [10 – 18]. We consider a nonstoichiometric compound $MX_y\square_{1-y}$ with a binary substitutional solution formed in its nonmetallic sublattice by the interstitial atoms X and vacancies □. In this solution, the atomic concentration of the component X is y and the total number of atoms and vacancies (or the number of sites of the nonmetallic sublattice) is N. If the coordination

number for the jth coordination sphere is equal to z_j, then the number of atoms X (or the number of occupied sites) is Ny, and the total number of sites on the jth coordination sphere centered at any atom X is $Nz_j y$. We let the respective numbers of atoms X and vacancies □ in the considered jth coordination sphere be denoted by $N^{(j)}_{(X)X}$ and $N^{(j)}_{(X)\square}$. The relative numbers of atoms X and vacancies on the jth coordination sphere are then given by

$$n^{(j)}_{(X)X} = \frac{N^{(j)}_{(X)X}}{Nz_j y} \quad \text{and} \quad n^{(j)}_{(X)\square} = \frac{N^{(j)}_{(X)\square}}{Nz_j y}\,.$$

In the case of the statistical distribution, the number of vacancies located on the jth coordination sphere centered at an atom X is $Nz_j y(1-y)$. In the presence of a short-range order, i.e., of correlations in the relative position of atoms, we have $N^{(j)}_{(X)\square} \neq Nz_j y(1-y)$; the following quantity is therefore introduced as a short-range order parameter that characterizes the relative deviation of the atomic distribution on the jth coordination sphere from the statistical distribution:

$$\alpha_j = \frac{Nz_j y(1-y) - N^{(j)}_{(X)\square}}{Nz_j y(1-y)} = 1 - \frac{n^{(j)}_{(X)\square}}{1-y}\,. \tag{1}$$

This is a short-range order parameter according to Cowley [14] and Warren [15]. If we choose the vacancy position □ as the center of the coordination sphere, we obtain a similar expression

$$\alpha_j = 1 - \frac{n^{(j)}_{(\square)X}}{y}\,. \tag{2}$$

Formulas (1) and (2) give the same value for the short-range order parameter. In the case of the statistical distribution, the quantities $n^{(j)}_{(X)\square}$ and $n^{(j)}_{(\square)X}$ obtained by averaging over all jth coordination spheres centered at atoms X and vacancies □ coincide with the respective concentrations $1-y$ and $\alpha_j = 0$; therefore, we have $\alpha_j < 0$. If, in the presence of correlations, the jth coordination sphere of an atom X predominantly contains vacancies, i.e., if $n^{(j)}_{(X)\square} > 1-y$ and $n^{(j)}_{(\square)X} > y$, then the short-range order parameter is negative ($\alpha_j < 0$). If the fraction of vacancies on the jth coordination sphere of an atom X is less than in the case of the statistical distribution, i.e., if $n^{(j)}_{(X)\square} < 1-y$ and $n^{(j)}_{(\square)X} < y$, then the short-range order parameter is positive ($\alpha_j > 0$). Thus, the sign of the short-range order parameter indicates the predominant character of the surroundings of an atom X on the jth coordination sphere with vacancies ($\alpha_j < 0$) or with atoms of the same sort ($\alpha_j > 0$).

In some cases, it is more suitable to use a short-range order parameter defined differently. Let the total number of atoms and vacancies (or the number of sites of the nonmetallic sublattice) be N. We consider a jth coordination sphere with a coordination number z_j. In the case of a statistical distribution, the numbers of pairs XX, X□, □X, and □□ of the same and of different sorts is determined by the binomial distribution and is equal to $N^{(j)} = Nz_j/2$. In the absence of short-range order, the number of pairs X□ and □X of different sorts on the jth coordination sphere is the same and is equal to

$$N^{\mathrm{bin}(j)}_{X\square} = N^{\mathrm{bin}(j)}_{\square X} = \frac{1}{2}\,Nz_j y(1-y)\,.$$

In the presence of short-range order, we have $N^{(j)}_{X\square} \neq N^{\mathrm{bin}(j)}_{X\square}$; therefore, the short-range order parameter is chosen as the quantity that characterizes the relative deviation of $N^{(j)}_{X\square}$ from $N^{\mathrm{bin}(j)}_{X\square}$, i.e.,

$$\alpha_j = 1 - \frac{N^{(j)}_{X\square}}{N^{\mathrm{bin}(j)}_{X\square}}\,. \tag{3}$$

Equation (3) is usually written in terms of the probabilities

$$P^{\mathrm{bin}}_{X\square} = \frac{N^{\mathrm{bin}(j)}_{X\square}}{N^{(j)}} \quad \text{and} \quad P^{(j)}_{X\square} = \frac{N^{(j)}_{X\square}}{N^{(j)}}$$

as

$$\alpha_j = 1 - \frac{P^{(j)}_{X\square}}{P^{\mathrm{bin}}_{X\square}}\,. \tag{4}$$

In describing a nonstoichiometric compound or a substitutional solid solution with a given composition and structural state, Eqns (1), (2), and (4) yield the same values of the short-range order parameter.

Relatively rarely, the short-range order parameter according to Bethe [13] is used:

$$\alpha^*_j = \frac{P^{(j)}_{X\square} - P^{\mathrm{bin}}_{X\square}}{P^{\mathrm{ord}(j)}_{X\square} - P^{\mathrm{bin}}_{X\square}}\,, \tag{5}$$

where $P^{\mathrm{ord}(j)}_{X\square}$ is the probability of formation, in a nonstoichiometric compound $MX_y\square_{1-y}y$ with the greatest possible long-range order, of pairs X□ with the spacing between the atom X and the vacant site equal to the radius of the jth coordination sphere. With this definition, the short-range order parameter α^*_j ranges from zero in the disordered nonstoichiometric compound ($P^{(j)}_{X\square} = P^{\mathrm{bin}}_{X\square}$) to unity in the ordered compound ($P^{(j)}_{X\square} = = P^{\mathrm{ord}(j)}_{X\square}$).

Along with short-range order parameters, frequently used in describing the structural state of a partially ordered nonstoichiometric compound are correlations ε defined [10] as the difference between the probability $P^{(1)(2)}_{X\square}$ of the formation of pairs X□ such that the atom X and the vacancy □ are located in different nonequivalent sublattices (e.g., in the 1st and 2nd sublattices) and the product of the type $P^{(1)}_X P^{(2)}_\square$:

$$\varepsilon^{(1)(2)}_{X\square}(R_j) = P^{(1)(2)}_{X\square} - P^{(1)}_X P^{(2)}_\square\,, \tag{6}$$

where R_j is the radius of the jth coordination sphere. The probabilities $P^{(1)}_X$ and $P^{(2)}_\square$ are uniquely defined through long-range order parameters, and correlation (6) makes it possible to more precisely describe the structural state of a partially ordered nonstoichiometric compound. In the general case, the correlations can be either positive or negative. In a completely ordered crystal, all correlations are zero, because the atomic distribution is exactly described by the long-range order parameters in this state.

In the absence of long-range order, short-range order is usually described by correlations defined as the difference of the probabilities for the detection of a pair X□ on the jth coordination sphere of a nonstoichiometric compound with a given structural state and of a disordered nonstoichiometric compound:

$$\varepsilon_{X\square}(R_j) = P^{(j)}_{X\square} - P^{\mathrm{bin}}_{X\square} = P^{(j)}_{X\square} - y(1-y)\,. \tag{7}$$

Because the pairs X□ and □X are equivalent, the pair correlations are equal to one another: $\varepsilon_{X\square}(R_j) = \varepsilon_{\square X}(R_j)$. In

the absence of long-range order, correlation function (7) tends to zero with increasing the radius R of the coordination sphere.

It follows from Eqns (4) and (7) that in the absence of long-range order, the short-range order parameter α_j and the pair correlations ε are related as

$$\varepsilon_{X\square}(R_j) = -y(1-y)\,\alpha_j\,,$$
$$\varepsilon_{XX}(R_j) = \varepsilon_{\square\square}(R_j) = y(1-y)\,\alpha_j\,. \tag{8}$$

It is obvious that all the above relations between the short-range order parameters and correlations are also completely applicable for substitutional solid solutions A_yB_{1-y}; in this case, we should only substitute A for X and B for $\square$ in these relations.

3. Effect of short-range order on the intensity of diffuse scattering

The disturbances of the ideal structure of a crystal that arise in the thermodynamic equilibrium can be regarded as fluctuations of some internal parameters. This allows describing the scattering of X-rays or neutrons from crystal-structure inhomogeneities as the scattering by fluctuation waves of composition or order parameters and related waves of static displacements of atoms. In particular, the method of fluctuation waves [16] permits one to account for the effects of correlations and short-range order in the relative position of atoms on the intensity of diffuse scattering.

In general, the intensity of scattering by a crystal can be presented as the sum

$$I(\mathbf{q}) = I_0(\mathbf{q})\exp(-2M) + I_{DAD}(\mathbf{q})\left[1-\exp(i2\pi\mathbf{q}\mathbf{u}_j)\right] + I_D(\mathbf{q})\,, \tag{9}$$

where $I_0(\mathbf{q})$ is the theoretical intensity of fundamental diffraction reflections in the absence of atomic displacements, $\mathbf{q}$ is the diffraction vector $\left(|\mathbf{q}| = (2\sin\theta)/\lambda\right)$, $\exp(-2M)$ is the factor that takes the weakening of the intensity of fundamental reflections due to static and dynamic (thermal) atomic displacements into account, $I_{DAD}(\mathbf{q})$ is the intensity of the diffuse background that arises due to displacements $\mathbf{u}_j$ of atoms from the regular crystal lattice sites, and $I_D(\mathbf{q})$ is the intensity of diffuse scattering caused by the difference in the atomic factors of scattering and by correlations (short-range order) in the relative position of atoms.

We consider the third term in Eqn (9) in more detail. This quantity $I_D(\mathbf{q})$ takes the effect of short-range order on the intensity of diffuse scattering into account.

Let the distribution of atoms in the crystal of a substitutional solid solution A_yB_{1-y} be characterized by occupation numbers $c(\mathbf{r})$ that take values 1 if the site $\mathbf{r}$ is occupied by an atom of sort A; if the site $\mathbf{r}$ is occupied by an atom of another sort, then $c(\mathbf{r}) = 0$. The atomic scattering factor corresponding to a certain site $\mathbf{r}$ can be represented as a superposition of atomic factors f_A and f_B at this site,

$$f(\mathbf{r}) = f_A c(\mathbf{r}) + f_B\left[1-c(\mathbf{r})\right]. \tag{10}$$

The scattering factor (10) for scattering by the site $\mathbf{r}$ includes a constant part and a variable part. Its constant part is the average atomic scattering factor equal to $\langle f\rangle = \sum_i f_i c_i$ (in the case under consideration, $\langle f\rangle = f_A c_A + f_B c_B$ or, with $c_A = y$ and $c_B = 1-y$, $\langle f\rangle = y(f_A - f_B) + f_B$). The variable part of the scattering power of the site $\mathbf{r}$, i.e., the fluctuation, is

$$\Delta f(\mathbf{r}) = (f_A - f_B)\left[c(\mathbf{r}) - y\right]. \tag{11}$$

According to [16], the intensity of diffuse scattering caused by the fluctuation in the scattering power of N sites can be written as

$$I_D(\mathbf{q}) = \sum_{j=0}^{N}\sum_{n=0}^{N}\Delta f(\mathbf{r}_n)\,\Delta f(\mathbf{r}_{n+j})\exp\left[i2\pi\mathbf{q}(\mathbf{r}_{n+j}-\mathbf{r}_n)\right]. \tag{12}$$

We select an arbitrary site $\mathbf{r}_n$ as the initial site with respect to which we consider correlations in the position of atoms, and assume that $\mathbf{r}_n = 0$. The vector $\mathbf{r}_{n+j} - \mathbf{r}_n$ that determines the position of any site of the crystal lattice relative to the initial site $\mathbf{r}_n$ is denoted by $\mathbf{R}_j$ (at $\mathbf{r}_n = 0$, we have $\mathbf{R}_j = \mathbf{r}_{n+j}$). We introduce the average quantity

$$\left\langle\Delta f(\mathbf{r}_n)\,\Delta f(\mathbf{r}_{n+j})\right\rangle = \frac{1}{N}\sum_{n=0}^{N}\Delta f(\mathbf{r}_n)\,\Delta f(\mathbf{r}_{n+j})\,. \tag{13}$$

With the adopted notation and with the substitution of Eqn (11) for fluctuations $\Delta f(\mathbf{r})$, Eqn (12) becomes

$$I_D(\mathbf{q}) = (f_A - f_B)^2 N\sum_{j=0}^{N}\left\langle\left[c(0)-y\right]\left[c(\mathbf{R}_j)-y\right]\right\rangle\exp(i2\pi\mathbf{q}\mathbf{R}_j). \tag{14}$$

Expression (14) can be decomposed into two components. The first is the term with $j = 0$ and the second is the sum taken over j from 1 to N (we note that $\mathbf{R}_j = 0$ at $j = 0$):

$$I_D(\mathbf{q}) = (f_A - f_B)^2 N\left\langle\left[c(0)-y\right]^2\right\rangle + (f_A - f_B)^2 N\sum_{j=1}^{N}\left\langle\left[c(0)-y\right]\left[c(\mathbf{R}_j)-y\right]\right\rangle \times\exp(i2\pi\mathbf{q}\mathbf{R}_j)\,. \tag{15}$$

Taking the equality $\langle c(\mathbf{r})\rangle = y$ and the identity $c^2(\mathbf{r}) \equiv c(\mathbf{r})$ into account, we have

$$\left\langle[c(0)-y]^2\right\rangle = \langle c^2(0)\rangle - 2y\langle c(0)\rangle + y^2 = y - 2y^2 + y^2 = y(1-y)\,;$$

therefore, the first component in (15) can be written as a Laue formula in the form

$$I_{DL}(\mathbf{q}) = Ny(1-y)(f_A - f_B)^2\,. \tag{16}$$

This component describes the Laue background, i.e., the contribution to the intensity of diffuse scattering that is independent of the degree of short-range order and is due to the difference in atomic scattering factors.

We now consider the second component of Eqn (15) in more detail. The factors $[c(0)-y]$ and $[c(\mathbf{R}_j)-y]$ describe excessive probabilities of occupation of the sites $\mathbf{r} = 0$ and $\mathbf{r} = \mathbf{R}_j$ by atoms of sort A; therefore, the average value of their

product is the correlation parameter $\varepsilon_{AA}(R_j)$:

$$\langle [c(0) - y][c(\mathbf{R}_j) - y] \rangle = \langle c(0)\, c(\mathbf{R}_j) \rangle - y^2 = \varepsilon_{AA}(\mathbf{R}_j)\,. \quad (17)$$

With (17), the second component in Eqn (15), i.e., the intensity of diffuse scattering caused by the substitutional short-range order, is equal to

$$I_{DSRO}(\mathbf{q}) = (f_A - f_B)^2 N \sum_{j=1}^{N} \varepsilon_{AA}(\mathbf{R}_j) \exp(i2\pi \mathbf{q}\mathbf{R}_j)\,. \quad (18)$$

According to Eqn (8), $\varepsilon_{AA}(R_j) = y(1-y)\alpha_j$. By substituting the short-range order parameter $\varepsilon_{AA}(R_j)$ for the correlation α_j in (18), we obtain

$$I_{DSRO}(\mathbf{q}) = y(1-y)(f_A - f_B)^2 N \sum_{j=1}^{N} \alpha_j \exp(i2\pi \mathbf{q}\mathbf{R}_j)\,. \quad (19)$$

The difference in the sizes of the substitutable atoms of a nonideal solid solution leads to displacements of atoms from their exact positions at the regular crystal lattice sites, i.e., to lattice distortions. In the presence of distortions, long-range elastic forces play a noticeable role. In nonideal solid solutions, the difference in the atomic radii of atoms of different sorts therefore affects the intensity of diffuse scattering both directly and indirectly. The direct effect is related to scattering by distortions; the indirect effects are due to the appearance of elastic energy that affects the probability of the appearance of fluctuations and thereby the diffuse scattering. As a result, the difference in atomic sizes leads to the occurrence in Eqn (19) of an additional exponential factor $\exp(-\beta_j)$ that reduces the intensity of diffuse scattering I_{DSRO} caused by short-range order. Taking the distortions into account is especially important if the lattice parameters strongly depend on concentration and if the atomic scattering factors f_A and f_B are close in magnitude. The problem of the effect of distortions on the intensity of diffuse scattering was considered in detail in [16].

Thus, the intensity of diffuse scattering from a single crystal caused by short-range order without taking static displacements of atoms into account is given by Eqn (19).

In those cases where the effect of static displacements can be neglected, an analysis of the intensity of diffuse scattering $I_D = I_{DL} + I_{DSRO}$ allows establishing the qualitative character of the substitutional short-range order. The diffuse scattering caused by a short-range order modulates the Laue background (Fig. 1). If the fraction of atoms of the same sort in the nearest neighborhood of an atom is greater in a solid solution than in the statistical distribution, then the short-range order parameter is positive ($\alpha_j > 0$). Therefore, at $\theta = 0$, the maximum positive contribution to I_D comes from local phase-separation effects due to short-range order, because the exponential factor $\exp(i2\pi\,\mathbf{q}\mathbf{R}_j) = \cos[4\pi R_j(\sin\theta)/\lambda] = 1$ at $\theta = 0$. With increasing θ and R_j, the exponential factor decreases rapidly to negative values and then again increases; however, with increasing R_j, the short-range order parameter α_j tends to zero, and therefore the contribution to the intensity of diffuse scattering decreases in absolute value (Fig. 1, curve *2*). If the nearest neighbors of atoms of a given sort are predominantly atoms of another sort ($\alpha_j < 0$), the contribution of the short-range order to the diffuse intensity I_D has the opposite sign relative to the contribution arising at $\alpha_j > 0$. The character of the variation

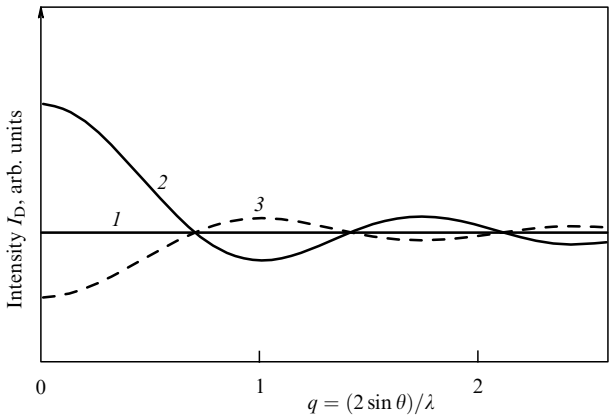

Figure 1. Effect of the structural state of a solid solution on the intensity $I_D = f(2\pi q)$ of the diffuse scattering of X-ray radiation or thermal neutrons ($q = (2\sin\theta)/\lambda$ is the diffraction vector): (*1*) diffuse scattering from a completely disordered ($\alpha_j = 0$) solid solution is due to only the Laue background; (*2*) the intensity of diffuse scattering in the case of local (short-range) phase separation ($\alpha_j > 0$); and (*3*) diffuse scattering in the case of short-range order ($\alpha_j < 0$).

of I_D upon short-range ordering ($\alpha_j < 0$) is shown in Fig. 1 (curve *3*).

For polycrystals, the intensity of diffuse scattering caused by a substitutional short-range order is described by an expression similar to (19), namely,

$$I_{DSRO}(\mathbf{q}) = y(1-y)(f_A - f_B)^2 N \sum_{j=1}^{\infty} \alpha_j z_j \frac{\sin 2\pi q R_j}{2\pi q R_j}\,. \quad (20)$$

The intensity of the Laue background I_{DL} for a polycrystalline binary solid solution is described by formula (16).

The curves of diffuse scattering of X-rays or neutrons allow finding the short-range order parameters α_j. To simplify calculations, the following function is usually considered:

$$Q(q) = \frac{I_{DSRO} + I_{DL}}{y(1-y)(f_A - f_B)^2 N} - 1 = \sum_{j=1}^{\infty} \alpha_j z_j \frac{\sin 2\pi q R_j}{2\pi q R_j}\,. \quad (21)$$

The simplest way to determine the parameters α_j from the measurements of $Q(q)$ is the use of the least-square method, i.e., solving a set of equations that relate the unknowns $x_j = \alpha_j z_j$ to given values of R_j and $Q(q_j)$, where $q_j = |\mathbf{q}_j|$ are the values of the diffraction vector at all points of the $Q(q)$ curve used for measurements.

Another method of calculating α_j amounts to the Fourier transformation of the $Q(q)$ function. We introduce a radial distribution function $U(R)$ that describes the deviation in the concentration of atoms of sort B in some coordination sphere of an atom A from the concentration of atoms of sort B in the same coordination sphere for the statistical distribution. This deviation is written as

$$\Delta n_j = \int_{R_j - \delta}^{R_j + \delta} U(R)\, dR\,. \quad (22)$$

On the other hand, $\Delta n_j = \alpha_j z_j$. Therefore,

$$\alpha_j z_j = \int_{R_j - \delta}^{R_j + \delta} U(R)\, dR\,. \quad (23)$$

It was shown in [2, 16] that the radial distribution function $U(R)$ can be written in terms of some arbitrary function $f(R)$ as $U(R) = (2R/\pi)\, f(R)$. Equation (23) then becomes

$$\alpha_j z_j = \frac{2R_j}{\pi} \int_{R_j-\delta}^{R_j+\delta} f(R)\, \mathrm{d}R\,. \tag{24}$$

The calculation of short-range order parameters using this method amounts to the following procedure: based on measured values of $Q(q)$, one constructs the $U(R)$ curve; according to (24), the area under this curve near the values of R_j gives the values of $\alpha_j z_j$. It is obvious that the $U(R)$ curve should have maxima only near R_j. A disadvantage of this method is that it does not allow resolving maxima with close values of the radii R_j and R_{j+1} of neighboring coordination spheres and calculating the corresponding short-range order parameters α_j and α_{j+1}.

As noted above, diffuse scattering can be a consequence of not only a substitutional short-range order but also dynamic (thermal) and static atomic displacements. Small static displacements can be due to the presence of point defects in the crystal. In crystals with a substitutional disorder, static atomic displacements arise because of the difference in the sizes of intersubstitutable atoms. These displacements lead to a modulation of diffuse scattering.

The authors of [19, 20] suggested a technique for analyzing experimental data on diffuse scattering that allows determining not only the short-range order parameters but also the static atomic displacements in different coordination spheres. According to Eqns (9), (15), (16), and (18), the intensity of diffuse scattering involves the Laue background I_{DL} and the respective contributions I_{DSRO} and I_{DAD} caused by the substitutional short-range order and atomic displacements. The contributions due to the short-range order and static displacements can be separated using the Sparks – Borie method [21]. The authors of [19, 20] modified this method and applied it to cubic nonstoichiometric compounds MX_y. According to [19, 20, 22], the intensity I_{DSRO} in an MX compound can be written as

$$I_{\mathrm{DSRO}} = \sum_{hkl} \alpha_{hkl} \cos\pi H_1 h \cos\pi H_2 k \cos\pi H_3 l\,, \tag{25}$$

where α_{hkl} is the short-range order parameter for the hkl coordination sphere with the radius $\mathbf{R}_{hkl} = h\mathbf{a}/2 + k\mathbf{b}/2 + l\mathbf{c}/2$ ($\mathbf{a}$, $\mathbf{b}$, and $\mathbf{c}$ are the basis vectors of the fcc unit cell) and H_1, H_2, and H_3 are the coordinates of the reciprocal-lattice points (we note that for a nonmetallic fcc sublattice, the sum $h + k + l = 2n$ is an even number, whereas for the metallic sublattice, $h + k + l = 2n + 1$ is an odd number). The intensity I_{DAD} in [19, 20] is expressed as a sum of two terms I_{AD1} and I_{AD2}. The first describes the modulation of the intensity of diffuse scattering caused by static size-effect-related atomic displacements and is equal to

$$\begin{aligned} I_{\mathrm{AD1}} &= H_1 Q_x(H_1, H_2, H_3) + H_2 Q_x(H_2, H_3, H_1) \\ &\quad + H_3 Q_x(H_3, H_1, H_2)\,, \end{aligned} \tag{26}$$

where

$$Q_x(H_1, H_2, H_3) = \sum_{hkl} \gamma_{hkl} \sin\pi H_1 h \sin\pi H_2 k \sin\pi H_3 l\,,$$

$$\gamma_{hkl} = -\pi \left[\frac{y}{1-y} + \alpha_{hkl} \right] \left\langle u^{hkl}_{\mathrm{X-X}} \right\rangle$$

if $h + k + l$ is even, and $\gamma_{hkl} = -[2\pi/(1-y)](f_{\mathrm{M}}/f_{\mathrm{X}})\, \langle u^{hkl}_{\mathrm{X-M}} \rangle$ if $h + k + l$ is odd; $\langle u^{hkl} \rangle$ is the relative displacement of two sites whose spacing is $\mathbf{R}_{hkl}$.

The second term accounts for the scattering from thermal vibrations of atoms and from displacements caused by point defects; it is written as

$$\begin{aligned} I_{\mathrm{AD2}} &= \sum_{hkl} \delta_{hkl} H_1^2 \cos\pi H_1 h \cos\pi H_2 k \cos\pi H_3 l \\ &\quad + \ldots + \sum_{hkl} \varepsilon_{hkl} H_1 H_2 \sin\pi H_1 h \sin\pi H_2 k \sin\pi H_3 l + \ldots\,, \end{aligned} \tag{27}$$

where δ_{hkl} and ε_{hkl} are coefficients related to atomic displacements. The second term I_{AD2} is much smaller than the first term I_{AD1}.

In a nonstoichiometric compound $\mathrm{MX}_y\square_{1-y}$, the short-range order parameter α_{hkl} can be determined through the probabilities of the formation of pairs 'vacancy $\square$ + interstitial atom X' ($P^{hkl}_{\mathrm{X-}\square}$ or $P^{hkl}_{\square-\mathrm{X}}$) by Eqns (1) or (2), which can be written as

$$\alpha_{hkl} = 1 - \frac{P^{hkl}_{\square-\mathrm{X}}}{y} \equiv 1 - \frac{P^{hkl}_{\mathrm{X-}\square}}{1-y}\,. \tag{28}$$

Hence, $P^{hkl}_{\square-\mathrm{X}} = y\,(1 - \alpha_{hkl})$. Because $P^{hkl}_{\mathrm{X-}\square} + P^{hkl}_{\mathrm{X-X}} = 1$, we have $P^{hkl}_{\mathrm{X-X}} = 1 - P^{hkl}_{\mathrm{X-}\square}$ or, taking (28) into account, $P^{hkl}_{\mathrm{X-X}} = 1 - (1-y)(1-\alpha_{hkl}) = y + (1-y)\,\alpha_{hkl}$. The displacements $\langle u^{hkl}_{\square-\mathrm{X}} \rangle$ and $\langle u^{hkl}_{\mathrm{X-X}} \rangle$ are related to the probabilities $P^{hkl}_{\square-\mathrm{X}}$ and $P^{hkl}_{\mathrm{X-X}}$ as

$$P^{hkl}_{\mathrm{X-X}} \langle u^{hkl}_{\mathrm{X-X}} \rangle + P^{hkl}_{\square-\mathrm{X}} \langle u^{hkl}_{\square-\mathrm{X}} \rangle = 0\,. \tag{29}$$

For a nonmetallic sublattice of an MX_y compound, the sum $h + k + l$ is an even number and we have

$$\gamma_{hkl} = -\pi \left(\frac{y}{1-y} + \alpha_{hkl} \right) \left\langle u^{hkl}_{\mathrm{X-X}} \right\rangle,$$

and therefore

$$\left\langle u^{hkl}_{\mathrm{X-X}} \right\rangle = -\frac{1-y}{\pi \left[y + (1-y)\,\alpha_{hkl} \right]}\, \gamma_{hkl}\,.$$

Substituting the values of $P^{hkl}_{\square-\mathrm{X}}$, $P^{hkl}_{\mathrm{X-X}}$, and $\langle u^{hkl}_{\mathrm{X-X}} \rangle$ in Eqn (29), we can find the root-mean-square static displacements in the nonmetallic sublattice as

$$\left\langle u^{hkl}_{\square-\mathrm{X}} \right\rangle = \frac{1}{2\pi(1-\alpha_{hkl})}\, \gamma_{hkl}\,. \tag{30}$$

The probabilities of the formation of the 'metal M – vacancy $\square$' and 'metal M + interstitial atom X' pairs in a nonstoichiometric compound MX_y are $P^{hkl}_{\mathrm{M-}\square} = 1 - y$ and $P^{hkl}_{\mathrm{M-X}} = y$. The probabilities $P^{hkl}_{\mathrm{M-}\square}$ and $P^{hkl}_{\mathrm{M-X}}$ are related to root-mean-square static displacements in the metallic sublattice $\langle u^{hkl}_{\square-\mathrm{M}} \rangle$ and $\langle u^{hkl}_{\mathrm{X-M}} \rangle$ as

$$P^{hkl}_{\mathrm{M-X}} \langle u^{hkl}_{\mathrm{X-M}} \rangle + P^{hkl}_{\mathrm{M-}\square} \langle u^{hkl}_{\square-\mathrm{M}} \rangle = 0\,. \tag{31}$$

For the metallic sublattice of the compound MX_y, the sum $h + k + l$ is an odd number and

$$\gamma_{hkl} = -\frac{2\pi}{1-y}\, \frac{f_{\mathrm{M}}}{f_{\mathrm{X}}}\, \left\langle u^{hkl}_{\mathrm{X-M}} \right\rangle,$$

and therefore

$$\langle u^{hkl}_{X-M} \rangle = -\frac{1-y}{2\pi}\frac{f_X}{f_M}\gamma_{hkl}.$$

Using this formula and the values of the probabilities $P^{hkl}_{M-\square}$ and P^{hkl}_{M-X}, we can transform Eqn (31) into an expression for determining the root-mean-square static displacements in the metallic sublattice of the MX_y compound as

$$\langle u^{hkl}_{\square-M} \rangle = \frac{y f_X}{2\pi f_M}\gamma_{hkl}. \quad (32)$$

In what follows, we consider experimental results on the short-range order and diffuse scattering of electrons and neutrons in nonstoichiometric compounds.

4. Diffuse scattering of neutrons and electrons in nonstoichiometric compounds

In the last few decades, numerous works concerning the investigation of short-range order in nonstoichiometric compounds by the methods of electron and neutron scattering have been published. The authors of [23, 24] used experimental results on the intensity of diffuse scattering of electrons from vanadium carbide $VC_{0.75}$ to calculate the short-range order parameters α_{hkl} for eight nearest coordination spheres (hkl) of its nonmetallic sublattice. As the center of coordination spheres, they selected a vacancy. For the nonstoichiometric carbide MC_y, the number of carbon atoms n_C and the number of vacancies $n_\square$ in the jth coordination sphere with a coordination number z_j are given by

$$n_C = z_j(1-\alpha_j)y, \quad n_\square = z_j\left[1-(1-\alpha_j)y\right]. \quad (33)$$

The results of the determination of the parameters α and of the number of carbon atoms n_C and vacancies $n_\square$ for each coordination sphere are given in Table 1. For comparison, the same parameters were calculated for the ordered phase V_6C_5 with a monoclinic (space group $C2/m$ or $C2/m$) or trigonal (space group $P3_1$) superstructures.

It can be seen from Table 1 that the distribution of carbon atoms and vacancies in the nonmetallic sublattice of the carbide $VC_{0.75}$ differs noticeably from the statistical distribution. For example, in the first two coordination spheres, the number of vacancies is far less than in the case of the statistical distribution. With increasing the coordination sphere radius, the value of α oscillates, gradually decreasing in absolute value. The authors of [23, 24] interpreted the results on the distribution of carbon atoms and vacancies as a consequence of mutual repulsion of vacancies and noted that an analogous short-range order should be observed in niobium and tantalum carbides. The conclusion on the similarity of short-range order in nonstoichiometric monocarbides of transition metals of Group V was also made in [26]. According to the authors of [26], it is impossible to obtain absolutely disordered (without short-range order) samples of vanadium carbide VC_y with $y > 0.78$.

A study of short-range order using diffuse scattering of neutrons from single crystals of $TiC_{0.76}$ and $NbC_{0.73}$ carbides was performed in [19]. The distribution of the intensity of diffuse scattering of neutrons was measured at the temperature 300 K in the $(1\bar{1}0)$ plane of the reciprocal lattice in the range of the diffraction vector variation $2 < 2\pi q < 40$ nm^{-1}. Before taking measurements, the $TiC_{0.76}$ and $NbC_{0.73}$ single crystals were annealed in a vacuum for several days. The obtained patterns of the diffuse scattering intensity are far from being periodic, which indicates the occurrence of displacements of atoms from the positions of the ideal nondistorted lattice. Using the Fourier transformation, the authors of [19] determined the short-range order parameters α for eight coordination spheres of the nonmetallic sublattice of the carbides $TiC_{0.76}$ and $NbC_{0.73}$ (see Table 1). As is seen from Table 1, the short-range order in titanium carbide is much weaker than in niobium carbide, but the distribution of vacancies is caused by their mutual repulsion, as in the case of vanadium carbide VC_y. According to [19], the correlations in niobium carbide extend to over more than nine coordination spheres. The results in [19] on the short-range order in niobium carbide agree qualitatively with analogous data in [27] obtained in studying powder samples of niobium carbide of compositions $NbC_{0.73}-NbC_{0.86}$ by the neutron diffuse scattering method.

The study of polycrystalline samples of $ZrC_{0.80}$ and $ThC_{0.75}$ by elastic neutron diffuse scattering permitted the authors of [26] to determine correlations in the distribution of vacancies in three coordination spheres (centered at a vacancy). According to [26], the cross sections of elastic diffuse scattering of neutrons for zirconium carbide $ZrC_{0.80}$ and thorium carbide $ThC_{0.75}$ are similar. In the $ThC_{0.75}$ carbide, there is a small number of vacancies (smaller than in the case of a statistical distribution) in the first coordina-

Table 1. Short-range order parameters α and the numbers of carbon atoms n_C and vacancies $n_\square$ in coordination spheres (hkl) of vanadium carbide $VC_{0.75}$, ideal ordered phase V_6C_5, and niobium and titanium carbides $NbC_{0.73}$ and $TiC_{0.76}$.

CS* (hkl)	CS** z_{hkl}	$VC_{0.75}$ [23]			V_6C_5 [23]			$NbC_{0.73}$ [19]			$TiC_{0.76}$ [19]		
		α	n_C	$n_\square$	α	n_C	$n_\square$	α	n_C	$n_\square$	α	n_C	$n_\square$
110	12	−0.178	10.6	1.4	−0.2	12	0	−0.095	9.6	2.4	−0.005	9.2	2.8
200	6	−0.260	5.7	0.3	−0.2	6	0	−0.275	5.6	0.4	−0.080	4.9	1.1
211	24	0.176	14.8	9.2	0.2	16	8	0.051	16.6	7.4	0.013	18.0	6.0
220	12	0.008	8.9	3.1	0	10	2	0.072	8.1	3.9	0.006	9.1	2.9
310	24	0.041	17.3	6.7	0	20	4	0.044	16.7	7.3	−0.003	18.3	5.7
222	8	−0.171	7.0	1.0	−0.2	8	0	−0.030	6.0	2.0	0.025	5.9	2.1
321	48	−0.070	38.5	9.5	−0.1	44	4	−0.020	35.7	12.3	−0.007	36.7	11.3
400	6	0.143	3.8	2.2	0.2	4	2	0.030	4.2	1.8	0.003	4.5	1.5

* CS is the coordination spheres (hkl) with the radius $R_j = (a_{B1}/2)(h^2+k^2+l^2)^{1/2}$, where a_{B1} is the lattice parameter of the disordered carbide MC_y with a structure of the $B1$ type; the coordination sphere is centered at a vacancy.

** CN is the coordination number for the coordination sphere (hkl).

tion sphere; in the second coordination sphere, the vacancies are completely absent; and in the third coordination sphere, the number of vacancies is greater than for the statistical distribution ($\alpha_1 = -0.05$, $\alpha_2 = -0.20$, $\alpha_3 = 0.075$). In the spectrum of zirconium carbide $ZrC_{0.80}$, there was also observed a wide diffuse maximum in the {1/2 1/2 1/2} reflection range, which is the first superlattice line in the spectrum of annealed zirconium carbide $ZrC_{0.64}$ (annealing was performed for 100 h at the temperature 1070 K).

A detailed study of short-range order in single crystals of $TiC_{0.64}$, $TiC_{0.76}$, $TiN_{0.82}$, $NbC_{0.73}$, and $NbC_{0.83}$ by elastic neutron diffuse scattering was performed by the authors of [20, 22, 28–32]. These investigations were undertaken as a continuation and development of works carried out in [19, 26, 33]. All the single crystals were obtained by the method of zone melting, which is described in detail in [34]. The single crystals of titanium and niobium carbides were obtained by zone melting of preliminarily sintered samples; the melting was performed in an atmosphere of pure helium under the pressure 2 MPa (20 atm). The single crystal of titanium nitride was obtained by zone melting of a titanium rod at the temperature 2870 K in the atmosphere of high-purity nitrogen; the nitrogen pressure was 2 MPa (20 atm). To perform neutron-diffraction studies, single-crystal samples in the form of cylinders about 10 mm in diameter and length were cut from the zone-melted rods. At the temperature 300 K, the respective lattice parameters a_{B1} of cubic single crystals of $TiC_{0.64}$, $TiC_{0.76}$, $TiN_{0.82}$, $NbC_{0.73}$, and $NbC_{0.83}$ were 0.4322, 0.4330, 0.4228, 0.4442, and 0.4453 nm.

The restoration of data on the short-range order parameters and atomic displacements from the intensities of diffuse scattering is a sufficiently complicated computational problem whose solution can involve significant errors. The magnitudes of the errors depend on the number of coordination spheres taken into account during the minimization, on the size of the zone selected near the diffraction reflection used (which affects the intensity of diffuse scattering), and on the calibration errors. To avoid these errors, the authors of [20, 22, 28–32] performed special investigations [22, 30] to estimate statistical computational errors. In particular, the direct minimization of experimental results for a vacancy placed in the center (000) of the coordination spheres yields a value for α_{000} that differs from the theoretical value by unity. This systematic error arises as a result of an uncertainty in the coefficients in the formula for the normalization of the elastic scattering cross section $d\sigma/d\Omega$. The corrected (taking into account that $\alpha_{000} = 1$) values of the short-range order parameters α_{hkl} were calculated by the formula

$$\alpha_{hkl}^{\text{corrected}} = \frac{1 + (d\sigma/d\Omega)_{\text{inc}}}{\alpha_{000}^{\text{noncorrected}} + (d\sigma/d\Omega)_{\text{inc}}}\ \alpha_{hkl}^{\text{noncorrected}}, \qquad (34)$$

where $(d\sigma/d\Omega)_{\text{inc}}$ is the incoherent scattering, which gives an additional weak contribution to the elastic scattering section. For the nonstoichiometric compounds MX_y, the magnitude of incoherent scattering is calculated (in Laue units) by the formula

$$\left(\frac{d\sigma}{d\Omega}\right)_{\text{inc}} = \frac{\sigma_{\text{M}}^{\text{inc}} + y\sigma_{\text{X}}^{\text{inc}} + \sigma_{\text{MX}}^{\text{dm}}}{y\,(1-y)\,\sigma_{\text{X}}^{\text{coh}}}, \qquad (35)$$

where σ^{coh} and σ^{inc} are the effective cross sections for the coherent and incoherent scattering and σ^{dm} is the cross section for multiple diffuse scattering (1 laue $= y\,(1-y)(f_{\text{X}})^2$, where f_{X} is the amplitude of coherent scattering of neutrons by an atom of sort X). For $TiC_{0.64}$, $TiC_{0.76}$, $TiN_{0.82}$, $NbC_{0.73}$, and $NbC_{0.83}$, the respective values of $(d\sigma/d\Omega)_{\text{inc}}$ are 0.26, 0.26, 0.29, 0.02, and 0.02 barn [20].

Table 2 lists the short-range order parameters for the nonmetallic sublattice of nonstoichiometric titanium and niobium carbides and for titanium nitride [20] corresponding to a quenched disordered state or to a disordered state that is in equilibrium at the temperature of measurement T, which is somewhat greater than the order–disorder transition temperature T_{trans} in these compounds. For comparison, the table also gives the short-range order parameters for the orthorhombic (space group $C222_1$) superstructure M_3X_2 and for the superstructures of the M_6X_5 type. Figure 2 shows the variation in the short-range order parameters in the $NbC_{0.73}$ carbide with increasing the radius $r = (a_{B1}/2)(h^2 + k^2 + l^2)^{1/2}$ of the coordination sphere (hkl).

The results in Table 2 allow making the following conclusions:

— in titanium carbide, an increase in the concentration of vacancies is accompanied by the extension of correlations to a greater number of coordination spheres; in $TiC_{0.76}$, the short-range order is already virtually absent in the fourth and subsequent coordination spheres, whereas in $TiC_{0.64}$, the correlations are retained up to the eighth coordination sphere (400);

— in all the samples studied, the short-range order parameters for the first (110) and second (200) coordination spheres are negative, and those for the third coordination sphere are positive. The α_{110}, α_{200}, and α_{210} parameters of the carbides $TiC_{0.76}$, $NbC_{0.73}$, and $NbC_{0.83}$ and of the nitride $TiN_{0.82}$ correspond best in sign and relative magnitude to the superstructure M_6X_5; for the carbide $TiC_{0.64}$, these parameters are closer to those of an orthorhombic superstructure (space group $C222_1$) of the M_3X_2 type;

— as is seen from the results for the $TiN_{0.82}$ nitride, all short-range order parameters decrease in the absolute value with increasing the temperature.

The investigations [20, 22, 28–32] of elastic neutron diffuse scattering show that a noticeable short-range order is retained in the nearest coordination spheres even at a temperature that is higher than the order–disorder temperature by 200–300 K. This indicates that the role of short-range interactions in nonstoichiometric compounds is very large. However, we cannot state that the short-range order in strongly nonstoichiometric compounds is exclusively due to the repulsion of vacancies. Such type of short-range order dominates in nonstoichiometric compounds $MX_y\square_{1-y}$y with the relative concentration of structural vacancies $1 - y \leqslant 0.3$. At a greater content of vacancies (e.g., in titanium carbide $TiC_{0.5}$–$TiC_{0.7}$), they cannot in principle be isolated from one another. In this case, there appears to arise a short-range order that is related to a clustering of vacancies into groups consisting of two, three, and a greater number of vacancies and to such a relative position of vacancy clusters that provides their greatest spacing.

The values of the coefficients γ_{hkl} and static displacements $\langle u_{\square-\text{M}}^{hkl}\rangle$ and $\langle u_{\square-\text{X}}^{hkl}\rangle$ determined in [20, 28–32] are given in Table 3. In calculating the displacements of metallic atoms $\langle u_{\square-\text{M}}^{hkl}\rangle$ via Eqn (32), we used the following neutron scattering amplitudes f_{M} and f_{X}: $f_{\text{Ti}} = -0.34 \times 10^{-12}$ cm, $f_{\text{Nb}} = 0.71 \times 10^{-12}$ cm, $f_{\text{C}} = 0.665 \times 10^{-12}$ cm, and $f_{\text{N}} = 0.94 \times 10^{-12}$ cm. The values of the displacements $\langle u_{\square-\text{M}}^{hkl}\rangle$ and $\langle u_{\square-\text{X}}^{hkl}\rangle$ in Table 3 are given in units $a_{B1} \times 10^{-4}/2$, where a_{B1} is the lattice parameter of the nonstoichiometric

Table 2. Short-range order parameters α_{hkl} in the nonmetallic sublattice of titanium and niobium carbides ($TiC_{0.64}$, $TiC_{0.76}$, $NbC_{0.73}$, $NbC_{0.83}$) and titanium nitride ($TiN_{0.82}$).

CS *	M_3X_2	$TiC_{0.64}$	$TiC_{0.76}$	$NbC_{0.73}$		$NbC_{0.83}$	M_6X_5
(*hkl*)	(space group $C222_1$)	1170 K **	1170 K **	Quenching ***	1470 K **	1470 K **	
000	1	1.000	0.934	1.000	1.000	1.000	1
110	−1/8	−0.055	−0.047	−0.085	−0.087	−0.063	−1/5
200	−1/2	−0.276	−0.122	−0.190	−0.196	−0.166	−1/5
211	1/8	0.037	0.035	0.088	0.072	0.094	1/5
220	1/4	0.088	0.018	0.039	0.018	0.005	0
310	1/8	0.021	−0.003	0.035	0.029	0.026	0
222	−1/8	−0.039	0.008	−0.044	−0.029	−0.019	−1/5
321	−3/16	−0.019	−0.001	−0.038	−0.024	−0.030	−1/10
400	0	0.072	0.009	0.010	0.010	0.009	1/5
330	0	0.001	0.010	0.009	−0.003	0.005	2/15
411	0	−0.014	−0.007	−0.022	−0.028	−0.035	2/15
420	0	−0.029	0.010	0.008	0.001	−0.001	−1/5
332	1/4	0.010	−0.002	0.031	0.006	0.002	0
422	0	0.016	−0.001	0.018	0.013	0.005	2/5
510	0	−0.010	−0.002	−0.002	−0.001	−0.011	−1/15
431	0	0.006	−0.003	0.007	0.002	−0.002	−1/15
521	1/8	0.009	0.000	0.003	0.000	0.000	0

CS *	M_3X_2	$TiN_{0.82}$				M_6X_5
(*hkl*)	(space group $C222_1$)	Quenching***	970 K**	1070 K**	1170 K**	
000	1	1.000	1.000	1.000	1.000	1
110	−1/8	−0.107	−0.101	−0.096	−0.091	−1/5
200	−1/2	−0.114	−0.114	−0.102	−0.096	−1/5
211	1/8	0.036	0.045	0.040	0.034	1/5
220	1/4	−0.002	0.018	0.013	0.013	0
310	1/8	0.004	0.019	0.016	0.014	0
222	−1/8	−0.041	−0.028	−0.023	−0.018	−1/5
321	−3/16	−0.025	−0.018	−0.015	−0.013	−1/10
400	0	−0.002	0.003	0.000	−0.005	1/5
330	0	0.012	−0.002	0.000	0.003	2/15
411	0	−0.019	−0.010	−0.008	−0.005	2/15
420	0	−0.005	0.003	0.004	0.004	−1/5
332	1/4	0.002	0.013	0.010	0.008	0
422	0	0.004	0.010	0.008	0.005	2/5
510	0	−0.005	−0.001	−0.001	−0.002	−1/15
431	0	−0.001	0.004	0.003	0.002	−1/15
521	1/8	−0.003	0.000	−0.001	−0.001	0

* CS — coordination sphere (*hkl*).

** Measurements were carried out on disordered samples at the specified temperature, which is somewhat higher than the order – disorder transition temperature T_{trans} in these compounds.

*** Measurements were conducted at 300 K on quenched disordered samples.

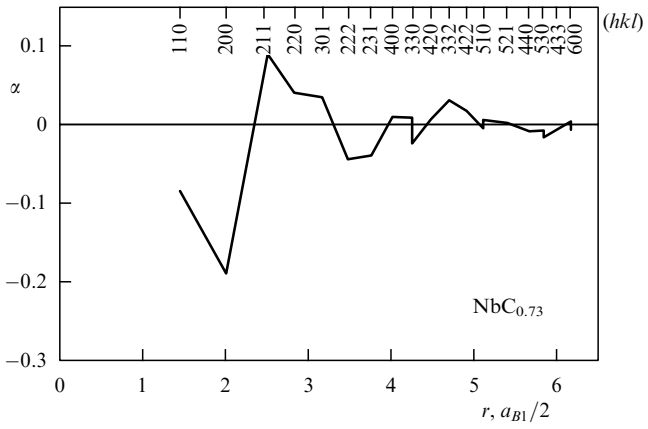

Figure 2. Short-range order parameters α_{hkl} in the disordered niobium carbide $NbC_{0.73}$ [22]; $r = (a_{B1}/2)(h^2 + k^2 + l^2)^{1/2}$ is the radius of the coordination sphere (*hkl*).

compounds under consideration, with the structure of the *B*1 (NaCl) type. The positive values of displacements mean that the atom moves away from the vacancy; negative displacements indicate that the atom approaches the vacancy.

As follows from Table 3, in the carbides studied ($TiC_{0.64}$, $TiC_{0.76}$, $NbC_{0.73}$, $NbC_{0.83}$) and in the nitride $TiN_{0.82}$, the metal atoms that are nearest to a vacancy move away from it, whereas the metal atoms of the next coordination sphere are displaced toward the vacancy.

In [35], the short-range order and long-range order in the metallic sublattices of carbide solid solutions $Ti_{0.95}V_{0.05}C_{0.21}$, $Ti_{0.95}V_{0.05}C_{0.55}$, $Ti_{0.75}V_{0.25}C_{0.21}$, and $Ti_{0.75}V_{0.25}C_{0.55}$ were studied using electron microscopy and electron diffraction. Solid-solution samples obtained by arc melting with a subsequent quenching of the melt contained two phases: a β phase (bcc solid solution of carbon in a β-(Ti,V) alloy) and a cubic δ phase (nonstoichiometric titanium carbide TiC_y

Table 3. Coefficients γ_{hkl} and root-mean-square static displacements $\langle u^{hkl}_{\square-M}\rangle$ and $\langle u^{hkl}_{\square-X}\rangle$ of metallic and nonmetallic atoms in titanium and niobium carbides ($TiC_{0.64}$, $TiC_{0.76}$, $NbC_{0.73}$, $NbC_{0.83}$) and titanium nitride ($TiN_{0.82}$) [20]; the displacements $\langle u^{hkl}\rangle$ are given in $a_{B1} \times 10^{-4}/2$ units.

Coordination sphere (hkl)	Pair □ – M or □ – X	$TiC_{0.64}$ $a_{B1} = 0.4332$ nm, 1170 K*		$TiC_{0.76}$ $a_{B1} = 0.4330$ nm, 1170 K*		$NbC_{0.73}$ $a_{B1} = 0.4442$ nm			
						Quenching**		1470 K*	
		γ_{hkl}	$\langle u^{hkl}\rangle$	γ_{hkl}	$\langle u^{hkl}\rangle$	γ_{hkl}	$\langle u^{hkl}\rangle$	γ_{hkl}	$\langle u^{hkl}\rangle$
100	□ – M	−0.127	253	−0.098	232	0.146	159	0.151	164
110	□ – X	−0.030	−45	−0.025	−38	−0.005	−7	0.001	1
111	□ – M	0.024	−48	0.017	−40	−0.047	−51	−0.063	−69
200	□ – X	0.034	42	−0.009	−13	−0.045	−60	−0.021	−28
102	□ – M	0.026	−52	0.004	−9	−0.007	−8	−0.005	−5
201	□ – M	0.004	−8	0	0	−0.015	−16	−0.022	−24
112	□ – X	0.008	13	0.006	10	0.002	3	0.002	3
211	□ – X	−0.002	−3	−0.002	−3	0.008	14	0.008	14
220	□ – X	−0.011	−19	0.001	2	0.008	13	0.012	19
122	□ – M	−0.007	14	0.004	−9	0.010	11	0.009	10
212	□ – M	0	0	0.002	−5	0.009	10	−0.003	−3
300	□ – M	0.028	−56	0.020	−47	−0.037	−40	−0.068	−74
103	□ – X	0.006	10	0.002	3	0.007	12	0.006	10
310	□ – X	0.003	5	0.002	3	0.010	16	0.013	21

Coordination sphere (hkl)	Pair □ – M or □ – X	$NbC_{0.83}$ $a_{B1} = 0.4453$ nm, 1470 K*		$TiN_{0.82}$ $a_{B1} = 0.4228$ nm					
				Quenching**		970 K*		1170 K*	
		γ_{hkl}	$\langle u^{hkl}\rangle$	γ_{hkl}	$\langle u^{hkl}\rangle$	γ_{hkl}	$\langle u^{hkl}\rangle$	γ_{hkl}	$\langle u^{hkl}\rangle$
100	□ – M	0.206	255	−0.049	177	−0.057	206	−0.051	184
110	□ – X	0.005	7	−0.015	−22	−0.025	−36	−0.027	−39
111	□ – M	−0.068	−84	0.021	−76	0.023	−83	0.024	−87
200	□ – X	−0.028	−38	0.016	23	0.022	31	0.022	32
102	□ – M	0.011	14	0.008	−29	0.011	−40	0.013	−47
201	□ – M	−0.020	−25	0.005	−18	−0.007	25	−0.009	32
112	□ – X	−0.004	−7	0.001	2	0.001	2	−0.002	−3
211	□ – X	0.001	2	−0.007	−12	0.007	12	0.008	13
220	□ – X	0.001	2	−0.003	−5	0.004	6	0.002	3
122	□ – M	0.010	12	−0.001	4	0	0	0.003	−11
212	□ – M	0.008	10	−0.001	4	−0.005	18	−0.003	11
300	□ – M	−0.061	−75	0.007	−25	−0.005	18	−0.005	18
103	□ – X	0.010	16	−0.002	−3	0.002	3	0.002	3
310	□ – X	−0.002	−3	0	0	0.008	13	0.009	15

* Neutron diffraction measurements were conducted on disordered samples at the specified temperature T.
** Neutron diffraction measurements were conducted at 300 K on quenched disordered samples.

with small impurity of vanadium). The respective samples of $Ti_{0.95}V_{0.05}C_{0.21}$, $Ti_{0.95}V_{0.05}C_{0.55}$, $Ti_{0.75}V_{0.25}C_{0.21}$, and $Ti_{0.75}V_{0.25}C_{0.55}$ contained 52.0, 97.2, 51.2, and 88.0 mol.% δ phases (of the respective composition $Ti_{0.997}V_{0.003}C_{0.493}$, $Ti_{0.985}V_{0.015}C_{0.570}$, $Ti_{0.991}V_{0.009}C_{0.519}$, and $Ti_{0.918}V_{0.082}C_{0.679}$). The precipitates of the δ phase were dendrites (up to 10 μm in size) surrounded with a matrix of the β-(Ti,V) alloy. The electron diffraction investigation of regions containing only the δ phase revealed additional periodic diffuse scattering and additional diffraction reflections not belonging to the δ phase. Both effects were related to the formation of a long-range order in the cubic TiC_y carbide. All additional reflections were superlattice ones and corresponded to the diffraction vector $\{1/2\ 1/2\ 1/2\}$. This indicates the formation of an ordered phase of the Ti_2C type in the titanium carbide studied. The small size of the domains of the ordered phase did not permit the authors of [35] to establish exactly to which space group ($R\bar{3}m$ or $Fd\bar{3}m$) this phase belongs.

An analysis of the diffuse scattering intensity permitted the authors of [35] to determine the short-range order parameters for eight coordination spheres of the nonmetallic sublattice of the cubic carbide phase (Table 4). The measured short-range order parameters α_{hkl} correlate well with the theoretical values of α calculated for the ideal ordered Ti_2C phase. The sign of α indicates that in the first and second coordination spheres of the nonmetallic sublattice, predominantly C–□ pairs are observed, whereas in the third coordination sphere, mainly C–C and □–□ pairs are observed. The introduction of corrections taking the width of diffuse diffraction reflections and the nonuniform distribution of intensity of these reflections into account permitted the authors [35] to substantially refine the experimentally found values of the short-range order parameters. To explain the results obtained, the authors of [35] used the concepts of the 'superlattice' and 'correlation' short-range order suggested in [36, 37]. According to the authors of [35], the

Table 4. Short-range order parameters α_{hkl} for the ordered phase of Ti_2C formed in cubic titanium–vanadium carbides $Ti_{0.997}V_{0.003}C_{0.49}$, $Ti_{0.991}V_{0.009}C_{0.52}$, and $Ti_{0.985}V_{0.015}C_{0.57}$ [35].

Coordination shell (*hkl*)	α_{exper}	α^*	α^{**}	α_{theor}
110	−0.183	−0.139	−0.117	0
200	−0.254	−0.147	−0.216	−1
211	0.189	0.083	0.070	0
220	−0.026	−0.009	0.046	1
310	0.050	0.013	0.011	0
222	−0.128	−0.025	0.052	−1
321	−0.089	−0.013	−0.011	0
400	0.171	0.019	0.034	1

Notes. α_{exper} are the experimental values of the short-range order parameters;
α^* are the corrected short-range order parameters calculated with the width of reflections taken into account (according to [35], these are the parameters of the correlation short-range order);
α^{**} are corrected short-range order parameters calculated with the nonuniform distribution of the reflection intensity taken into account (according to [35], these parameters include correlation and superstructure short-range order simultaneously);
α_{theor} are theoretical short-range order parameters for the ideal ordered Ti_2C phase (space group $R\bar{3}m$ or $Fd\bar{3}m$).

short-range order parameters α^* corrected for the width of reflections characterize only the correlation short-range order, whereas the parameters α^{**} calculated with the nonuniform intensity distribution taken into account include the superlattice and correlation components simultaneously. We note that the superlattice parameter α_{000} for the cubic and trigonal ordered Ti_2C phases is identically equal to zero, whereas according to [35], the α_{000} parameter is negative both without corrections (α_{exper}) and with corrections (α^*, α^{**}). It can be supposed that these discrepancies are due to some factors related to scattering by vanadium atoms present in the diffraction regions studied and to static displacements of atoms that have not been taken into account in [35].

In [38], the short-range order in lower hexagonal carbides of vanadium and niobium (V_2C_y and Nb_2C_y) was studied using electron diffuse scattering. The investigation showed that the short-range order and long-range order in these carbides were related to a specific distribution of carbon atoms and structural vacancies, which formed regular C–□–C–□–... chains parallel to the *c*-axis. A comparison of the experimental and calculated values of the diffuse scattering intensity permitted the authors of [38] to establish the possible types of ordering in V_2C and Nb_2C.

The investigation of electron diffraction in the cubic monoxide TiO_y ($1.00 \leqslant y \leqslant 1.25$) [39] also revealed the presence of diffuse scattering, but no quantitative characteristics of the short-range order were given in the paper. Measurements of the X-ray diffraction diffuse scattering from single-crystal disordered titanium monoxide $TiO_{0.997}$ at 1323K [40] showed a tendency for the nearest neighborhood of titanium atoms to contain vacancies in both the metallic and oxygen sublattices. This follows from the negative sign of the short-range order parameters $\alpha_{Ti-□}$ and $\alpha_{Ti-■}$ for the nearest coordination spheres formed around Ti atoms by the sites of both oxygen and titanium sublattices (□ and ■ are here the respective vacancies in the nonmetallic and metallic sublattices). According to [40], the short-range order in $TiO_{0.997}$ corresponds to the atomic distribution characteristic of the ordered monoclinic phase Ti_5O_5.

5. Short-range order in carbide solid solutions

The method of X-ray diffraction diffuse scattering was repeatedly employed to study short-range order in the metallic sublattice of solid solutions formed by transition-metal carbides. According to [17], the most substantial results of studying short-range order in $M^{(I)}C-M^{(II)}C$ solid solutions are that a nonchaotic distribution of metal atoms over the sites of the metallic sublattice was established and the effect of carbon on the correlations in the distribution of metallic atoms was detected.

The local distribution of atoms was first fixed in the metallic sublattice of NbC–TaC and ZrC–HfC equimolar solid solutions [41–43]. The absence of vacancies in the carbon sublattice and the proximity of the atomic radii of the substitutable metals (Nb and Ta; Zr and Hf) suggest that no static distortions are present in the lattice of these solid solutions. The short-range order parameters for the three nearest coordination spheres in the metallic sublattice were determined from the diffuse scattering intensity $I_D = I_{DL} + I_{DSRO}$ (the intensities I_{DL} and I_{DSRO} were described by Eqns (16) and (20), in which the atoms A and B were taken to be the substitutable metallic atoms). The short-range order parameters in the first and second coordination sphere proved to be positive; the magnitudes of both α_1 and α_2 increased with decreasing the temperature of quenching or annealing (Table 5). The positive values of α_1 and α_2 indicate that in these solid solutions, in the first and second coordination spheres nearest to a metal atom of a given sort, the concentration of metal atoms of the same sort is greater than for the statistical distribution. In other words, a short-range separation exists in the metallic sublattice of NbC–TaC and ZrC–HfC solid solutions. The local (short-range) phase separation is also observed in metallic Nb–Ta alloys [44]. The short-range order parameter α_3 for the third coordination sphere is negative and close to zero; therefore, we can assume that the correlations in the distribution of atoms of the metallic sublattice extend only over the two nearest coordination spheres. An additional annealing of the samples at a reduced temperature and the introduction of 1 mol.% WC into the solid solution led to an increase in correlations in the relative position of metallic atoms.

In [45, 46], the authors studied diffuse scattering of X-rays by solid solutions such as $Ti_{0.5}Nb_{0.5}C$, $Ti_{0.5}Ta_{0.5}C$, $Ti_{0.5}W_{0.5}C$, $V_{0.5}Nb_{0.5}C$, and $V_{0.5}W_{0.5}C$, and by metallic alloys such as $Ti_{0.5}Ta0.5$, $V_{0.64}Nb_{0.36}$, and $V_{0.65}W_{0.35}$. The short-range order parameter α_1 for the $Ti_{0.5}Ta_{0.5}$ alloys proved to be positive; that for the $V_{0.64}Nb_{0.36}$ and $V_{0.65}W_{0.35}$ alloys was negative; and for the $V_{0.5}W_{0.5}C$, we have $\alpha_1 > 0$. In carbide solid solutions $Ti_{0.5}Nb_{0.5}C$, $Ti_{0.5}Ta_{0.5}C$, and $V_{0.5}W_{0.5}C$, the sign of the short-range order parameter α_1 changes to the opposite compared with the alloys Nb_xTi_{1-x} [47], $Ti_{0.5}Ta_{0.5}$, and $V_{0.65}W_{0.35}$.

Short-range order in TiC–WC solid solutions was studied in [48–50]. Measurements of X-ray diffuse scattering were performed on samples of various compositions subjected to various heat treatments (sintering at various temperatures, quenching, cooling with a furnace, etc.). According to the results obtained, all samples of TiC–WC solid solutions with a complete (without vacancies) carbon sublattice revealed a noticeable short-range order in the first coordination sphere ($\alpha_1 < 0$); the short-range order parameters α_2 and α_3 for the second and third coordination spheres were close to zero (Table 5). This means that the correlations in the position of

Table 5. Short-range order parameters α_1, α_2, and α_3 for the first, second, and third coordination spheres of the metallic sublattice of a carbide solid solution and alloys.

Composition	Heat treatment	α_1	α_2	α_3	References
$Nb_{0.5}Ta_{0.5}C$	Annealing, 2000 K	0.058	0.025	0	[41]
$Nb_{0.5}Ta_{0.5}C$	Annealing, 1800 K	0.089	0.049	0	[41]
$Nb_{0.5}Ta_{0.5}C$	Annealing, 1500 K	0.120	0.071	0	[41]
$Nb_{0.5}Ta_{0.5}C + 1$ mol.% WC	Annealing, 1800 K	0.11	0.10	0.02	[43]
$Nb_{0.5}Ta_{0.5}C + 1$ mol.% WC	Annealing, 1500 K	0.14	0.13	0.04	[43]
$Nb_{0.5}Ta_{0.5}$	Quenching, 1600 K	0.13	0.09	0.02	[44]
$Nb_{0.5}Ta_{0.5}$	Annealing, 1400 K	0.16	0.08	−0.04	[44]
$Zr_{0.5}Hf_{0.5}C$	Quenching, 2200 K	0.06	0	0	[42]
$Zr_{0.5}Hf_{0.5}C$	Quenching, 1800 K	0.09	0	0	[42]
$Nb_{0.5}Ti_{0.5}C$	Quenching, 2200 K	−0.06	—	—	[17, 45, 46]
$Nb_{0.75}Ti_{0.25}$	Quenching, 1500 K	0.066	0.103	—	[47]
$Nb_{0.5}Ti_{0.5}$	Quenching, 1500 K	0.063	0.047	—	[47]
$Nb_{0.25}Ti_{0.75}$	Quenching, 1500 K	0.091	0.017	—	[47]
$Ti_{0.5}Ta_{0.5}C$	Quenching, 2200 K	−0.06	—	—	[17, 45, 46]
$Ti_{0.5}Ta_{0.5}$	Quenching, 1500 K	0.19	—	—	[17, 45, 46]
$Ti_{0.5}Zr_{0.5}C$	Quenching	0.07	—	—	[17]
$Ti_{0.6}Hf_{0.4}C$	Quenching	0.03	—	—	[17]
$V_{0.5}Nb_{0.5}C$	Quenching, 2100 K	−0.01	—	—	[17, 45, 46]
$V_{0.64}Nb_{0.36}$	Quenching	−0.23	—	—	[17, 45, 46]
$V_{0.5}W_{0.5}C$	Quenching, 2100 K	0.03	—	—	[17, 45, 46]
$V_{0.65}W_{0.35}$	Quenching	−0.10	—	—	[17, 45, 46]
$Ti_{0.5}W_{0.5}C$	Quenching, 2200 K	−0.06	—	—	[17, 45, 46]
$Ti_{0.61}W_{0.39}C_{0.98}$	Quenching, 2400 K	−0.09	0.03	0	[48]
$Ti_{0.77}W_{0.23}C_{0.98}$	Quenching, 2400 K	−0.07	0	0	[48]
$Ti_{0.84}W_{0.16}C_{0.98}$	Quenching, 2400 K	−0.06	0.02	0.01	[48]
$Ti_{0.91}W_{0.09}C_{0.98}$	Quenching, 2400 K	−0.06	−0.02	−0.02	[48]
$Ti_{0.58}W_{0.42}C_{0.94}$	Quenching, 2400 K	−0.06	0.04	0	[48]
$Ti_{0.58}W_{0.42}C_{0.86}$	Quenching, 2400 K	0.05	0.16	0.04	[48]
$Ti_{0.59}W_{0.41}C_{0.78}$	Quenching, 2400 K	0.07	0.15	0.03	[48]

titanium and tungsten atoms exist at small distances (within one to three coordination spheres). In all cases, an additional annealing of the samples at a reduced temperature led to an increase in the short-range order parameters. No state with a distribution of metallic atoms close to the statistical one has been fixed.

An increase in the content of tungsten in TiC – WC solid solutions is accompanied by an increase in the degree of short-range order in the first coordination sphere. The distribution of metallic atoms is affected quite strongly by the concentration of carbon. With a deviation from the stoichiometric composition in carbon, the short-range order parameters in all three coordination spheres become positive (Table 5). At the same time, the specific features of X-ray diffuse scattering by nonstoichiometric solid solutions $Ti_xW_{1-x}C_y$ led the authors of [48] to a supposition of the existence of two types of short-range orders, with $\alpha_1 < 0$ and $\alpha_1 > 0$, in the structure of a solid solution. In this connection, the authors of [48] suggested that in the nonstoichiometric solid solution $Ti_xW_{1-x}C_y$, regions of the short-range order with a structure typical of a stoichiometric solid solution are retained along with the formation of segregates of atoms of the same sort.

6. Diffuse scattering and the cluster model of substitutional short-range order

The predominant surrounding of atoms of a given sort by atoms of a certain sort in disordered solid solutions is a short-range-order effect. In diffraction experiments, the presence of a short-range order leads to the appearance of three-dimensional regions of diffuse-scattering intensity in reciprocal space. Generally, the intensity maxima are located at strictly definite crystallographic positions. For example, in fcc solid solutions, these maxima lie in the regions of reciprocal space with coordinates of the type (100), (1/2 1/2 1/2), (1 1/2 0), etc. [51].

In passing into an ordered state, the intensity of diffuse scattering gradually becomes concentrated in positions corresponding to superlattice reflections. The state of the crystal at a temperature that is somewhat higher than the order – disorder transition temperature, i.e., the state in which there is a certain short-range order but no long-range order has yet appeared, is considered [23, 25, 51 – 55] as a 'transition state.' The transition state is characterized by the presence of well-outlined contours of diffuse intensity in the diffraction pattern. Such a state of an orderable solid solution or of a nonstoichiometric compound can be described in terms of the cluster model [51] developed in [52 – 55]. This model was first suggested in [56] to explain the distribution of intensity of diffuse scattering in the compound $LiFeO_2$ with a substitutional short-range order. Later [23], this model was successfully applied for analyzing substitutional short-range order in orderable nonstoichiometric carbides and nitrides MX_y. In [57], the cluster model [51] was used to estimate the relationship between the short-range order parameters in the two nearest coordination shells of an fcc solid solution $A_{0.5}B_{0.5}$.

6.1 Diffuse-intensity contours in the cluster model

According to [53], the locus $f(\mathbf{g})$ of the diffuse intensity contours correlates with the existence in the crystal of relatively small polyhedral clusters of a definite type that can have one or several configurations. By the type of cluster, we mean the number of lattice sites belonging to the cluster and their spatial arrangement. The cluster configuration is determined by how many atoms of different sorts (A and B in the case of an A_yB_{1-y} solid solution) or interstitial atoms X

and vacancies □ (in the case of a nonstoichiometric compound MX_y ($MX_y\square_{1-y}$)), and in which order with respect to one another, are located at the sites belonging to the cluster. In general, the cluster type and its configuration are determined by the crystal lattice symmetry and the composition y of the ordering crystal. With progressing ordering, i.e., with the transition from a disordered into an ordered state, a redistribution of atoms over the lattice sites occurs and some of the possible types and configurations of clusters become predominant. As a result, the intensity of diffuse scattering in some regions of the three-dimensional reciprocal lattice becomes stronger such that contours of diffuse intensity (flat sections of the three-dimensional distribution of diffuse intensity) occur in the diffraction pattern. At the final stage of ordering, the intensity of diffuse scattering is entirely concentrated in superlattice reflections. If there are clusters of several types or configurations in the ordered crystal, the positions of superlattice reflections coincide with the sites of mutual intersection of regions of diffuse scattering related to different clusters.

Let

$$f(\mathbf{g}) = 0 \tag{36}$$

(where $\mathbf{g}$ is the vector of the reciprocal lattice) be the equation that describes the locus of the contours of the diffuse scattering region in the reciprocal lattice. Because the intensity of diffuse scattering must have the translational symmetry of the reciprocal lattice, Eqn (36) can be represented as a Fourier sum,

$$f(\mathbf{g}) = \sum_k \omega_k \exp(-\mathrm{i}2\pi\mathbf{g}\mathbf{r}_k) = 0\,, \tag{37}$$

where $\mathbf{r}_k$ are the lattice vectors and ω_k are the Fourier coefficients. If the intensity of diffuse scattering is localized inside the contour described by Eqn (36), the function $f(\mathbf{g})$ is related to the amplitude $F_\mathrm{D}(\mathbf{g})$ of diffuse scattering by the identity

$$f(\mathbf{g})\, F_\mathrm{D}(\mathbf{g}) \equiv 0\,, \tag{38}$$

which means that the amplitude and the intensity $I_\mathrm{D}(\mathbf{g}) = |F_\mathrm{D}(\mathbf{g})|^2$ of diffuse scattering can differ from zero only along the contour defined by Eqn (36). According to [54, 55], the amplitude of diffuse scattering for a binary solid solution A_yB_{1-y} can be written as

$$F_\mathrm{D}(\mathbf{g}) = \left[f_\mathrm{A}(\mathbf{g}) - f_\mathrm{B}(\mathbf{g})\right] \sum_j \sigma_j \exp(\mathrm{i}2\pi\mathbf{g}\mathbf{r}_j)\,, \tag{39}$$

where σ_j is the scalar occupation operator ($\sigma_j = -(1-y)$ if the site j is occupied by an atom of sort A and $\sigma_j = y$ if the site j is occupied by an atom of sort B). Identity (38) and the explicit form of the amplitude $F_\mathrm{D}(\mathbf{g})$ in (39) allow obtaining a system of homogeneous linear equations for all sites j:

$$\sum_k \omega_k \sigma_{j+k} = 0\,. \tag{40}$$

The relation of type (40) describes the structure of a cluster in which the positions of sites are determined by vectors $\mathbf{r}_j + \mathbf{r}_k$, where $k = 0, 1, 2, \ldots$. In the ideal case, it is valid for all polyhedral clusters defined by the $\mathbf{r}_k$. The simplest interpretation of this cluster relation corresponds to the case where all the coefficients in Eqn (40) are equal to unity or zero ($\omega_k = 1$, $\sum_k \sigma_{j+k} = 0$). This means that all the clusters under consideration have the same composition coinciding with the average composition of the crystal. But in reality, cluster relation (40) differs somewhat from zero, because in a real structure, while being valid for an arbitrarily chosen cluster, it may prove to be invalid for a neighboring cluster. The minimum deviations from zero are provided by clusters whose existence probability in the structure under consideration is greatest; it is for these clusters that the intensity of diffuse scattering is localized in the locus determined by Eqn (36). Thus, it is obvious that the cluster model in [51–55] cannot completely describe an ordered state.

The real use of an approximate cluster model of a transition state typically amounts to the simulation of the surface of diffuse intensity for a given cluster, the calculation of the shape of sections of the simulated surface by various planes, and the comparison of the sections obtained with experimentally observed diffraction patterns containing the maxima of the diffuse intensity distribution. In simulating the surface of diffuse scattering by a cluster including n sites, the function $f(\mathbf{g})$ is defined as an exponential sum over all cluster sites:

$$f(\mathbf{g}) = \sum_{j=1}^{n} \exp\left[\mathrm{i}2\pi(h_j + k_j + l_j)\right] = 0\,. \tag{41}$$

As a natural cluster that corresponds to the geometry of the fcc lattice and allows simulating diffuse-intensity contours for compounds with an orderable fcc lattice, a tetrahedron consisting of four sites, an octahedron of six sites, or a cube of eight sites can be used (Fig. 3).

We first consider the simulation of diffuse scattering using an octahedral cluster. The sites of the octahedron have the coordinates $(h/2\ 0\ l/2)$, $(h/2\ k/2\ 0)$, $(0\ k/2\ l/2)$, $(h/2\ k\ l/2)$, $(h/2\ k/2\ l)$, and $(h\ k/2\ l/2)$. According to (41) and to the coordinates of the octahedron sites, we obtain the following exponential form of the equation describing the contour of

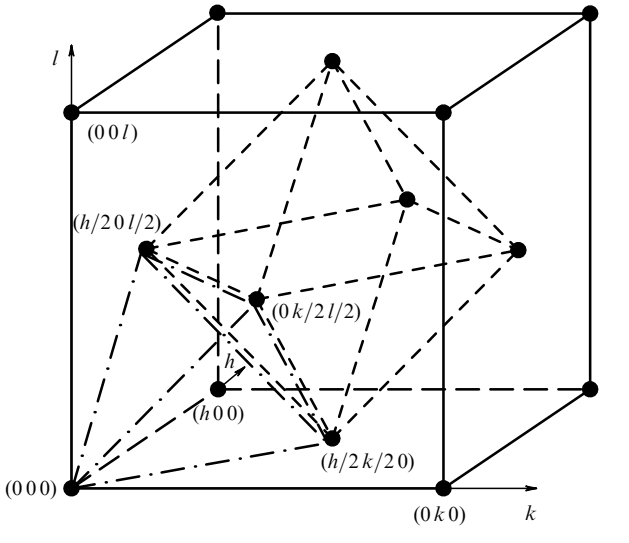

Figure 3. Types of clusters in the fcc lattice used for the description of the diffuse scattering surface: a tetrahedron formed by four sites (dot-and-dashed lines); an octahedron formed by six sites (dashed lines); and a cube formed by eight sites (solid lines).

the diffuse scattering region for an octahedral cluster:

$$f(\mathbf{g}) = \exp\left[\mathrm{i}\pi(h+l)\right] + \exp\left[\mathrm{i}\pi(h+k)\right] + \exp\left[\mathrm{i}\pi(k+l)\right] + \exp\left[\mathrm{i}\pi(h+2k+l)\right] + \exp\left[\mathrm{i}\pi(h+k+2l)\right] + \exp\left[\mathrm{i}\pi(2h+k+l)\right] = 0\,. \quad (42)$$

After standard transformations, Eqn (42) can be written in the trigonometric form

$$\cos\pi h + \cos\pi k + \cos\pi l = 0\,. \quad (43)$$

The sites of a cubic cluster have the coordinates (000), (h00), (0k0), (00l), (hk0), (h0l), (0kl), and (hkl) (see Fig. 3). For these sites, the function in (41) is $f(\mathbf{g}) = \cos\pi h \times \cos\pi k \cos\pi l$ and the equation that describes the surface of the diffuse scattering region has the form

$$\cos\pi h\,\cos\pi k\,\cos\pi l = 0\,. \quad (44)$$

For a tetrahedral cluster (see Fig. 3) with sites (000), (h/2 k/2 0), (h/2 0 l/2), and (0 k/2 l/2), we have

$$f(\mathbf{g}) = 1 + \exp\left[\mathrm{i}\pi(h+k)\right] + \exp\left[\mathrm{i}\pi(h+l)\right] + \exp\left[\mathrm{i}\pi(k+l)\right]\,. \quad (45)$$

The tetrahedral cluster was used in [54] to analyze the experimental results in [39] on the diffraction of electrons in titanium monoxide. The surface of the diffuse scattering region in titanium monoxide TiO_y ($1.00 \leqslant y \leqslant 1.25$) was described in [54] by the function

$$f(\mathbf{g})f^*(\mathbf{g}) - C = 0\,, \quad (46)$$

where $f(\mathbf{g})$ is given by Eqn (45), $f^*(\mathbf{g})$ is the complex conjugate function, and C is a numerical parameter close in magnitude to unity and only weakly dependent on the composition of the titanium monoxide. After standard transformations, Eqn (46) reduces to the trigonometric form

$$\cos\pi h\,\cos\pi k + \cos\pi h\,\cos\pi l + \cos\pi k\,\cos\pi l + \left(1 - \frac{C}{4}\right) = 0\,. \quad (47)$$

In Eqns (42)–(45) and (47) describing the position of the diffuse scattering contour, the indices h, k, and l are the coordinates in the reciprocal lattice.

Diffuse-scattering contours for nonstoichiometric compounds MX_y (titanium monoxide, vanadium carbide, and titanium nitride) were first observed [25, 39] in diffraction patterns obtained by electron diffraction. An analysis of the experimental data in [25] on the diffuse scattering of electrons from ordering vanadium, niobium, and tantalum carbides and titanium nitride, which was performed in [23], showed that the shape of the diffuse scattering region is more precisely described by the function

$$(\cos\pi h + \cos\pi k + \cos\pi l) - C\cos\pi h\,\cos\pi k\,\cos\pi l = 0\,, \quad (48)$$

which combines Eqns (43) and (44). The parameter C in Eqn (48) depends on the nature and composition of the compound under consideration; for example, for cubic carbides, nitrides, and MX_y oxides, it varies from 0 to 3; in complex lithium oxides $Li_{1-x-z}\square_y M_{1+x}O_2$, the parameter C changes from 6 to 10. It is obvious that the description of the diffuse scattering surface by Eqn (48) in fact means the use of a unit cell of the fcc lattice as the model cluster.

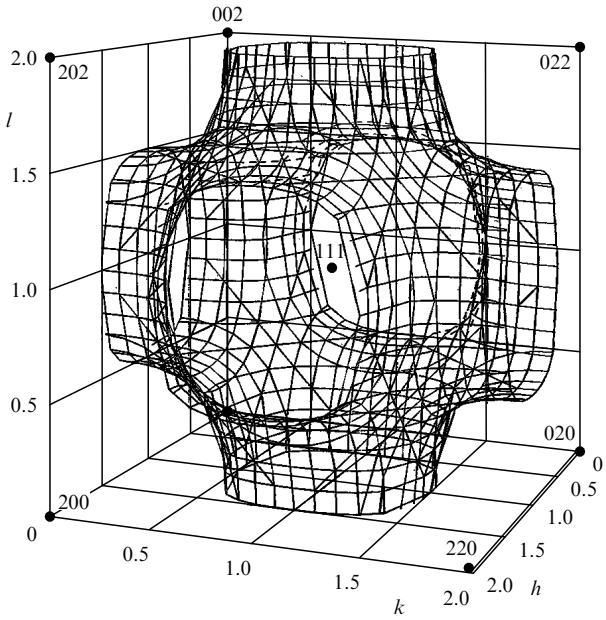

Figure 4. Distribution of the diffuse scattering intensity contours in the reciprocal lattice of fcc crystals corresponding to model (48) at $C = 3$ (schematic), and (●) the positions of the reciprocal-lattice points. With a decrease in the parameter C to zero, when the diffuse scattering is simulated by only an octahedral cluster and is described by Eqn (43), the shape of the surface changes insignificantly.

The calculated form of the three-dimensional distribution of the diffuse scattering intensity for the fcc lattice described by Eqn (48) at $C = 3$ is shown in Fig. 4. It is seen that the model diffuse scattering surface resembles the Fermi surface of simple metals. The question about a correlation between diffuse scattering and the topology of the Fermi surface was first raised in [39]. Somewhat later, this was noted by the authors of [23], who constructed a three-dimensional model of the diffuse scattering surface in the reciprocal lattice of the fcc crystal based on the experimental electron-diffraction data [25]; they noted that the diffuse scattering surface is very close in shape to the theoretical Fermi surface of cubic metals [58] with 1 electron per atom.

We consider the shape of the section of the diffuse scattering contour by the (001) plane of the reciprocal lattice of an ordered fcc crystal. Let the diffuse scattering contour be described by Eqn (48). For the section by the planes of the (001) family, l in Eqn (48) is an integer; therefore, $\cos\pi l \equiv \pm 1$. For odd l, Eqn (48) acquires the form

$$\cos\pi h + \cos\pi k + \cos\pi l - C\cos\pi h\,\cos\pi k\,\cos\pi l = \cos\pi h + \cos\pi k - 1 + C\cos\pi h\,\cos\pi k = 0\,, \quad (49)$$

and hence, $\cos\left[\cos\pi k(1 + C\cos\pi h)\right] = (1 - \cos\pi h)$ and

$$k = \pm\frac{1}{\pi}\,\arccos\frac{1-\cos\pi h}{1+C\cos\pi h} + 2m\,, \quad (50)$$

where $m = 0, \pm 1, \pm 2, \pm 3, \ldots$ is an integer coefficient that takes the periodicity of the arc trigonometric function into account. In the particular case where $C = 0$, we obtain the

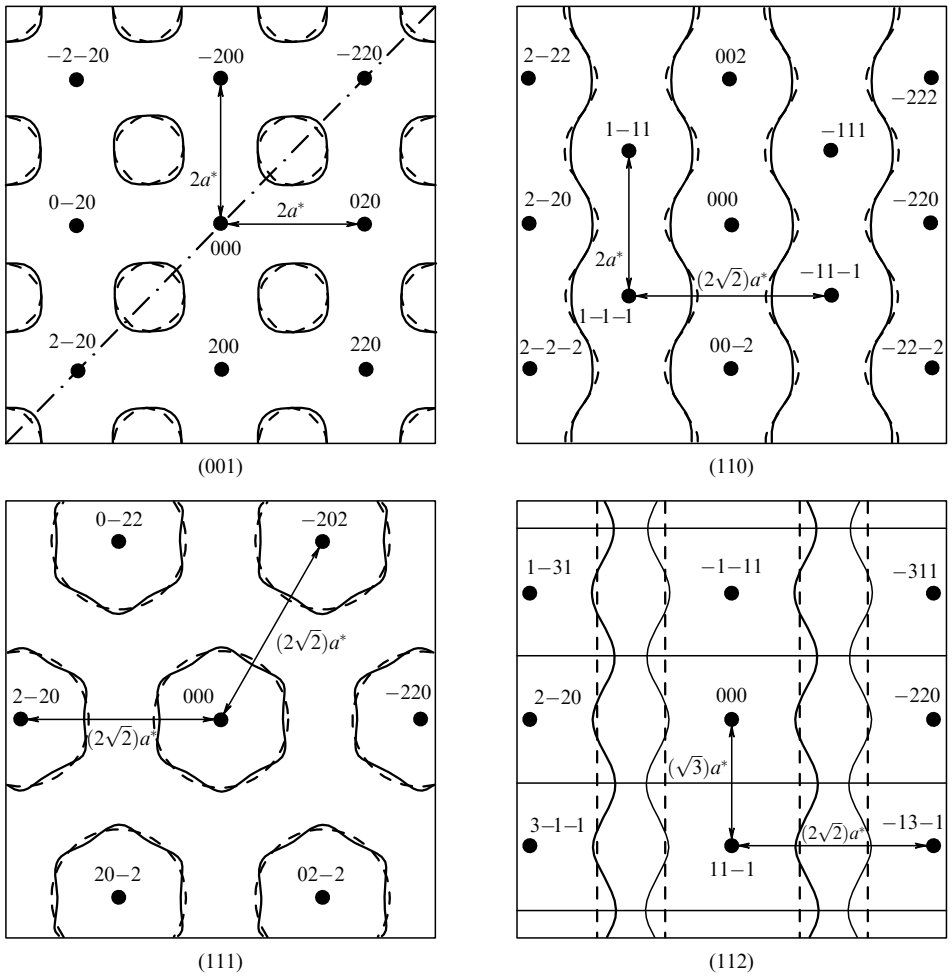

Figure 5. Sections of the diffuse scattering intensity surface [described by Eqn (48)] by the (00*l*) plane at even values of *l* (at odd *l*, the sections have the same shape but are shifted by the vector {110}) and by the (110), (111), and (112) planes of the reciprocal lattice of the fcc crystal. Solid lines correspond to sections at $C = 3$, with the unit cell of the fcc lattice (a combination of octahedral and cubic clusters) used as a model cluster. Dashed lines correspond to sections of the surface at $C = 0$, when the diffuse scattering surface is simulated using only an octahedral cluster and is described by Eqn (43), which is a particular case of Eqn (48). In the (112) section, the horizontal lines of the contour exist at any value of the parameter *C*.

section of diffuse scattering contour (43) by the (001) plane:

$$k = \pm\frac{1}{\pi}\,\arccos(1 - \cos\pi h) + 2m\,. \tag{51}$$

It can be easily understood from Fig. 4 that at odd ($l = 2n - 1$) and even ($l = 2n$) values of *l*, the sections of the diffuse scattering contour by the (001) plane have the same shape but are displaced with respect to one another by the vector {110}. The sections of the diffuse scattering contours described by Eqn (48) by (00*l*) planes of the reciprocal lattice are shown in Fig. 5.

Sections of the diffuse scattering contour by other planes of the reciprocal lattice can be constructed similarly. For example, in constructing sections of the contour by the (110) plane, we should find a solution of Eqn (48) at $h + k = 2n$, where $n = 0, \pm1, \pm2, \pm3, \ldots$. It is obvious that in this case, $\cos\pi k = \cos(2\pi n - \pi h) \equiv \cos\pi h$; therefore, Eqn (48) becomes

$$\begin{aligned}&\cos\pi h + \cos\pi k + \cos\pi l - C\cos\pi h\,\cos\pi k\,\cos\pi l\\ &\quad = 2\cos\pi h + \cos\pi l - C\cos^2\pi h\,\cos\pi l = 0\,,\end{aligned} \tag{52}$$

whence we have

$$h_{1,2} = \pm\frac{1}{\pi}\,\arccos\frac{2 \pm \sqrt{4 + 4C\cos^2\pi l}}{2C\cos\pi l} + 2m \tag{53}$$

or

$$l = \pm\frac{1}{\pi}\,\arccos\left(-\frac{2\cos\pi h}{1 - C\cos^2\pi h}\right) + 2m\,. \tag{54}$$

If $C = 0$, then solving Eqn (43) gives

$$l = \pm\frac{1}{\pi}\,\arccos(-2\cos\pi h) + 2m\,. \tag{55}$$

The respective sections of diffuse scattering surfaces (48) and (43) by the (110) plane of the reciprocal lattice that were calculated by Eqns (54) and (55) are shown in Fig. 5. Determining the section of the diffuse scattering contour by the (111) plane passing through the origin amounts to solving Eqn (48) under the condition $h + k + l = 0$. The solution is rather unwieldy:

$$\begin{aligned}h_{1,2} &= \pm\frac{1}{\pi}\,\arccos Y_{1,2} - \frac{l}{2} + 2m\,,\\ k_{1,2} &= -(h_{1,2} + l)\,,\end{aligned} \tag{56}$$

where

$$Y_{1,2} = \frac{2\cos(\pi l/2) \pm \sqrt{4\cos^2(\pi l/2) - 2C[C\cos\pi l - C - 2]\cos^2\pi l}}{2C\cos\pi l}\,.$$

If $C = 0$, the section of the contour by the (111) plane is described by the equation

$$h = \pm\frac{1}{\pi}\arccos\left(-\frac{\cos\pi l}{2\cos(\pi l/2)}\right) - \frac{l}{2} + 2m\,,$$

$$k = -(h + l)\,. \qquad (57)$$

Finally, we consider the section of the diffuse scattering contour by the (112) plane. In this case, Eqn (48) has two solutions under the condition $h + k + 2l = 0$:

$$h_{1,2} = \pm\frac{1}{\pi}\arccos\left(\frac{1}{C} \pm \sqrt{\frac{2 + 2C + C^2 - C^2\cos 2\pi l}{2C^2}}\right) - l + 2m\,,$$

$$k_{1,2} = -(h_{1,2} + 2l) \qquad (58)$$

and

$$l = \pm\frac{1}{2} + 2m\,. \qquad (59)$$

If $C = 0$, Eqn (48) is transformed into Eqn (43); in this case, the first solution becomes

$$h = \pm\frac{2}{3} - l + 2m\,, \qquad k = -(h + 2l)\,, \qquad (60)$$

and the second solution retains its form (59).

The sections of diffuse scattering by (111) and (112) planes of the reciprocal lattice calculated via Eqns (56)–(60) at $C = 0$ and $C = 3$ are shown in Fig. 5.

According to [23], the parameter C in Eqn (48), which determines the shape of the diffuse scattering contours, can be determined from the experimental pattern of diffuse scattering as

$$C = \frac{1 + 2\cos 2\pi F}{3\cos^2 2\pi F}\,, \qquad (61)$$

where $F = [D_{(000-220)} - D_{\text{diff}}]/2D_{(000-220)}$, $D_{(000-220)}$ is the distance between the fundamental reflections (000) and (220), and D_{diff} is the distance between diffuse bands located between the (000) and (220) reflections.

6.2 Electron diffraction and diffuse scattering of compounds with a short-range order

We consider some experimental results on diffuse scattering in nonstoichiometric compounds with the substitutional short-range order as compared to those obtained in model calculations. Figure 6 displays electron diffraction patterns obtained in [54] from crystals of cubic ($B1$-type structure) lithium ferrite $LiFeO_2$ in sections (001), (110), and (111) of the reciprocal lattice. The diffuse scattering in $LiFeO_2$ is due to the inverse substitution of Fe^+ and Fe^{3+} ions. The experimentally observed diffuse scattering contours were successfully described by model (48) with the cubic unit cell of the fcc lattice used as the model cluster. For $LiFeO_2$, the best agreement is reached when the parameter C in Eqn (48) is equal to 8 (or $6 \leqslant C \leqslant 10$) [54]. Indeed, the schemes of the corresponding sections of the diffuse scattering surface (see Fig. 5) calculated via Eqn (48) at $C > 0$ agree well with the experimental diffuse scattering contours (Fig. 6).

The model of the transition state has been successfully applied for an analysis of diffuse scattering (Fig. 7) found in electron-microscopic investigations of the complex lithium oxide $LiFe_{0.6}Ni_{0.4}O_2$ with substitution of Fe and Ni atoms [59]. This compound, just like lithium ferrite, has a cubic structure of the $B1$ type. Electron diffraction from samples of $LiFe_{0.6}Ni_{0.4}O_2$ in sections (110) and (111) of the reciprocal lattice, along with fundamental reflections of the $B1$ lattice, revealed a system of periodic curved diffuse features that do not pass through the sites of the reciprocal lattice of the cubic solid solution and are characteristic of the substitutional short-range order in orderable solid solutions. To simulate the diffuse scattering distributions in reciprocal space, the authors of [59] used an octahedral cluster and described the diffuse scattering surface in the first approximation by Eqn (43). However, the shape of the diffuse scattering contours is such that it can best be described by Eqn (48) obtained using a model cluster in the form of a cubic unit cell of the fcc lattice. An analysis of the diffuse intensity redistribution performed for the possible types of short-range orders suggests that the short-range order observed in $LiFe_{0.6}Ni_{0.4}O_2$ precedes the formation of a rhombohedral (space group $R\bar{3}m$) superstructure.

Diffuse scattering related to the formation of the substitutional short-range order in the defect iron sublattice of the complex sulfide $Fe_{0.25}NbS_2$ ($Fe_{0.25}\square NbS_2$) was revealed in [60]. The short-range order in this compound arises as a result of a redistribution of iron atoms and structural vacancies. The appearance of diffuse effects was explained in terms of the

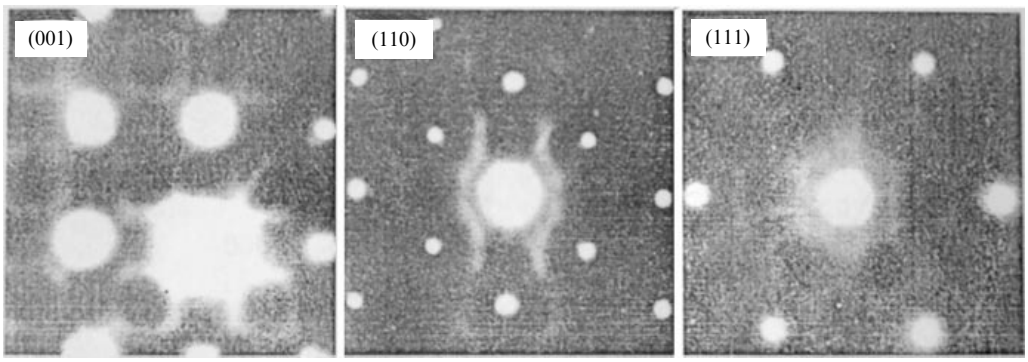

Figure 6. Experimental electron diffraction patterns from a cubic ($B1$ type) lithium ferrite LiFeO2 [54] in sections (001), (110), and (111) of the reciprocal lattice.

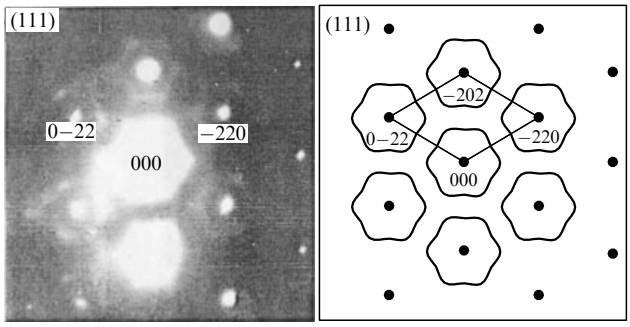

Figure 7. Diffraction pattern obtained from crystals of a cubic ($B1$ type) solid solution $LiFe_{0.6}Ni_{0.4}O_2$ in the section (111) of the reciprocal lattice, and the corresponding key pattern of this section [59]. The diffuse scattering surface is described by Eqn (43) corresponding to the use of an octahedral model cluster.

transition state model [52–54]. The diffuse scattering contours are distinctly seen in the electron diffraction pattern in the (001) section of the reciprocal lattice (Fig. 8). A diffuse intensity enhancement is observed in those places of the contours that correspond to the positions of the reciprocal lattice where superlattice reflections should arise upon the formation of a long-range order.

In [61, 62], electron diffraction was used to study short-range order in complex carbides $Ti_{0.80}Mo_{0.17}V_{0.03}C_x$ (for brevity, the authors of [61, 62] have written their formula as (Ti, Mo)C_x or $(Ti_{0.8}Mo_{0.2})C_x$). This carbide solid solution with a substitution of Ti and Mo atoms in the metallic sublattice has a cubic structure of the $B1$ type. It was revealed in a nickel-base superalloy containing (at. %) ~ 59.2 Ni, 9.2 Cr, 12.6 Co, 1.7 Mo, 5.4 Ti, 11.1 Al, 0.7 C, 0.07 B, and

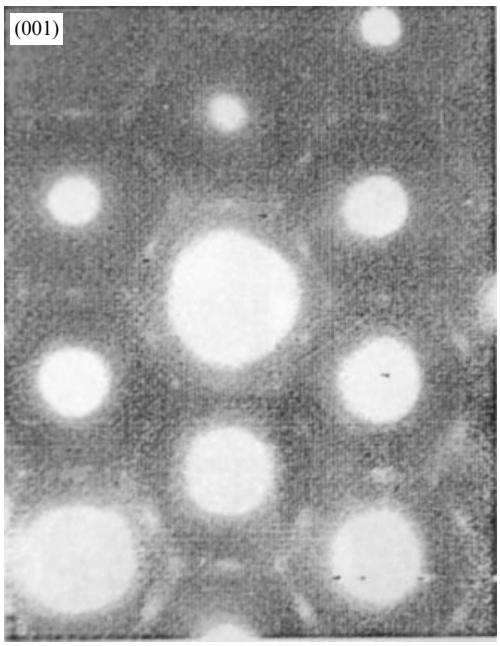

Figure 8. Electron diffraction pattern from the cubic ($B1$ type) complex sulfide $Fe_{0.25}\square NbS_2$ [60] in the (001) section of the reciprocal lattice. Along with fundamental reflections, diffuse scattering maxima are seen in those regions of reciprocal space where superlattice reflections arise due to the formation of a long-range order.

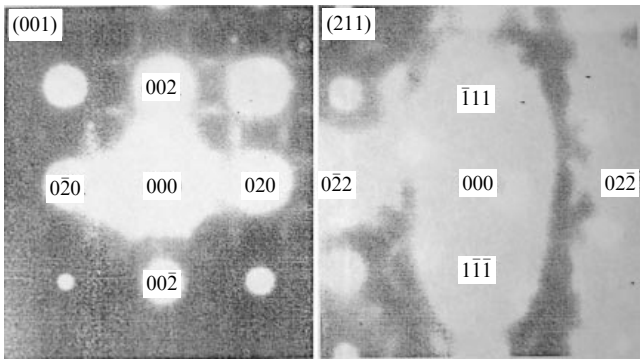

Figure 9. Diffuse scattering in the (001) and (211) sections of the reciprocal lattice of cubic ($B1$ type) carbide solid solutions (Ti, Mo)C_x [61].

0.02 Zr. The electrolytic dissolution of the alloy in a mixture of several acids permitted the authors to extract (Ti, Mo)C_x single crystals 5–20 μm in size from this alloy, which were used for the investigation.

Diffuse scattering in (Ti, Mo)C_x samples was observed in the sections (001) and (211) (Fig. 9) and was absent in the section (110) of the reciprocal lattice. In the diffraction pattern of the (001) section, the diffuse scattering regions represent lines extended in the [010] and [001] directions. The diffuse scattering maxima correspond to equivalent positions (1 1/2 0) and do not form rings similar to those observed earlier [25] for the nonstoichiometric vanadium carbide VC_y. The diffuse intensity maxima in positions (1/2 1/2 0) that were observed in [63] for the nonstoichiometric niobium carbide NbC_y are also absent in (Ti, Mo)C_x. The diffuse scattering distribution in the (211) section of the reciprocal lattice of the carbide solid solution (Ti, Mo)C_x is similar to that for the Ni_4Mo alloy exhibiting a short-range order [64] and analogous alloys Au_4Cr, Au_4V, and Au_4Fe. If the diffuse scattering in (Ti, Mo)C_x is due to a redistribution of carbon atoms and vacancies, then it should also be observed in all section of the reciprocal lattice; however, no diffuse scattering was observed experimentally in the (110) section. This fact and the similarity of the diffuse scattering in (Ti, Mo)C_x and in the Ni_4Mo and Au_4M alloys (M = Cr, V, Fe) gave grounds to the authors of [61] to arrive at the following conclusion: the short-range order in a carbide solid solution (Ti, Mo)C_x is related to a redistribution of Ti and Mo atoms in the metallic fcc sublattice that precedes the formation of an ordered tetragonal body-centered structure of the Ti_4Mo in this sublattice.

An additional confirmation of the fact that the diffuse effects observed in (Ti, Mo)C_x are due to short-range order in, precisely, the metallic rather than in the carbon sublattice are the results in [62] on irradiation of this carbide solid solution with high-energy electrons. After irradiation of (Ti, Mo)C_x samples with 125 keV electrons, the diffuse scattering remained unaltered, although a similar irradiation of an ordered vanadium carbide V_8C_7 led to the complete disappearance of superlattice reflections. This agrees with the results in [65], where the disordering of the carbide V_6C_5 was caused by irradiation with 100 keV electrons. In the V_8C_7 and V_6C_5 carbides, the ordering is related to a redistribution of carbon atoms and structural vacancies. The diffuse scattering in (Ti, Mo)C_x samples disappeared only after irradiation with electrons with the energy 2 MeV. According to the estimation made in [62], the energy of electrons required to ensure

shifting metal atoms Ti and Mo should exceed 1 MeV, which agrees with experimental results. Thus, the diffuse scattering in carbide solid solutions (Ti, Mo)C_x is due to the short-range order in the metallic sublattice.

In recent work [66], electron diffraction was used to study short-range order in the nonstoichiometric zirconium nitride ZrN_y. The sample of ZrN_y was obtained using a 2 h annealing of an α-Zr foil 50 μm thick in nitrogen at 1470 K. Then, the sample was subjected to a homogenizing annealing at the same temperature for 10 h in an argon atmosphere followed by quenching. The content of nitrogen in the nitride foil was 31.9 at.%; the sample was two-phase; it contained α-Zr along with the cubic ($B1$ type) nitride ZrN_y. It is obvious that the chemical composition of the zirconium nitride studied in [66] and the concentration of structural vacancies in the nitrogen sublattice of this nitride are still not exactly known. Because the sample was two-phase, the composition of the zirconium nitride was most probably close to the lower boundary of the homogeneity region, i.e., to $ZrN_{0.5-0.6}$. For investigations using electron microscopy (in a JEOL 2000FXII device with the working voltage 200 keV), the regions of the foil were selected that contained zirconium nitride. Electron diffraction patterns were obtained using various orientations of the sample; to reveal weak reflections, the exposure time was made sufficiently long (90 – 180 s).

In [66], patterns of the diffuse scattering intensity distribution in four sections of the reciprocal lattice of an fcc crystal, namely (001), (011), (111), and (112), have been obtained; for example, Fig. 10 shows diffuse scattering in the (001) and (111) sections. The shape of the diffuse scattering contours obtained in [66] for ZrN_y corresponds to the model described by Eqn (48). An estimation of the parameter C by Eqn (60) yields $C = 0.45$, which is close to the value found in [23] for titanium nitride TiN. Along with the diffuse intensity contours corresponding to model (48), the authors of [66] revealed diffuse intensity maxima in the (001) section in the position (1 1/2 0) and other equivalent positions. We note that the superlattice vector [1 1/2 0] belongs to the star $\{\mathbf{k}_8\}$ of the Brillouin zone of the fcc lattice [2]. Earlier, diffuse intensity maxima in such positions were observed in the solid solution (Ti, Mo)C_x [61, 62], which exhibits ordering of the Ti_4Mo type in the metallic sublattice; no such maxima were found experimentally in cubic monocarbides and mononitrides MX_y. According to [66], the appearance of diffuse intensity maxima in ZrN_y in positions (1 1/2 0) can be due to ordering into a tetragonal structure of the M_2X (space group $I4_1/amd$) or M_4X_3 (space group $I4/mmm$) type. Indeed, the channel of the order – disorder transition related to the formation of superstructures includes rays of the star $\{\mathbf{k}_8\}$ [1, 2] to which the superlattice vector [1 1/2 0] belongs. Based on the possible composition of the zirconium nitride and the absence of intensity maxima in the (100) positions (which should be present in the case of a tetragonal ordering of the M_4X_3 type), ordering of the M_2X type (space group $I4_1/amd$) is more probable in the zirconium nitride ZrN_y studied in [66]. Thus, the authors of [66] in fact supposed that the intensity maxima observed in positions of the (1 1/2 0) type are low-intensity superlattice reflections that correspond to an ordered phase with a small degree of long-range order.

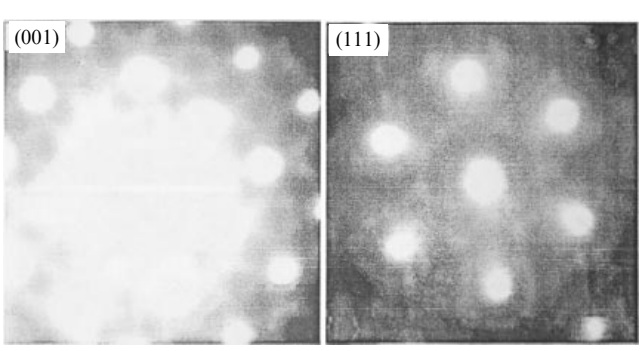

Figure 10. Diffuse scattering in the (001) and (111) sections of the reciprocal lattice of the cubic ($B1$ type) zirconium nitride ZrN_y [66].

To clarify whether the intensity maxima (1 1/2 0) observed in ZrN_y are related to the ordering of the N atoms and nitrogen vacancies, the sample studied was subjected to electron irradiation in situ, in the column of an electron microscope. The irradiation with 200 keV electrons for 600 s led to a weakening of the diffuse scattering intensity in positions (1 1/2 0), and irradiation for 3000 s led to its complete disappearance. According to the authors of [66], the observed disordering is not a consequence of heating the sample, because zirconium nitride ZrN_y has a high thermal conductivity and its heating with an electron beam does not exceed several degrees kelvin, i.e., is negligible. The authors of [66] believe that a more likely cause of disordering can be related to displacements of N atoms as a result of collisions with high-energy electrons. The maximum energy E_t^{max} transferred by electrons to atoms during irradiation can be estimated [67] by the formula that describes the elastic collisions of particles with relativistic effects taken into account,

$$E_t^{max} = \frac{2E(E+2mc^2)}{Mc^2}, \qquad (62)$$

where E is the energy of irradiating electrons, m is the electron mass, M is the mass of the irradiated atom, and c is the speed of light. Atomic displacements occur if the transferred energy E_t^{max} is greater than the displacement threshold T_d. The displacement threshold is the minimum energy that is sufficient to displace an atom from its position in the crystal lattice. It follows from Eqn (62) that for electrons with the energy $E = 200$ keV, the maximum energies E_t^{max} transferred to Zr and N atoms in the zirconium nitride ZrN_y are 5.7 and 37.4 eV, respectively (in [66], it is erroneously indicated that $E_t^{max} = 17.2$ eV for nitrogen atoms). The authors of [66] supposed that the displacement threshold for an N atom in ZrN_y is close in magnitude to the displacement threshold for carbon C in vanadium carbide V_6C_5 ($VC_{0.83}$), equal to 5.4 eV [65]. If so, we have $E_t^{max} > T_d$ for N atoms in zirconium nitride. We note that this estimate of the displacement threshold for N atoms in ZrN_y appears to be a minimum and possibly underestimated. Indeed, if, according to [62], the displacement threshold for carbon atoms T_d^C in carbides of transition metals is about 5 eV, then, according to [68], we have the displacement threshold $T_d^C = 4-16$ eV for the $TiC_{0.97}$ and $TaC_{0.99}$ carbides, whereas the investigation in [69] showed that $TaC_{0.99}$ $T_d^C = 23.2 \pm 1.1$ eV in tantalum carbide $TaC_{0.99}$. According to various estimates [62, 65, 68 – 71], the displacement threshold for metallic atoms in monocarbides and mononitrides of transition metals is 20 – 50 eV ($T_d^{Ta} = 42$ eV in tantalum carbide [69] and $T_d^U = 27 \pm 1$ eV in uranium nitride [71]); in general, therefore, T_d^M is greater than the displacement threshold for nonmetallic interstitial

atoms. Because $E_t^{max} > T_d$ for zirconium nitride, the authors of [66] made the following conclusion. The disappearance of intensity maxima in positions (1 1/2 0) upon irradiation of zirconium nitride with 200 keV electrons occurs as a result of disordering caused not by heating the sample with the electron beam but by displacements of nitrogen atoms from their positions in the ordered structure in the course of electron bombardment.

In the examples considered, the electron diffraction method was used to observe diffuse scattering related to only the substitutional short-range order. The authors of [72–74] revealed short-range orders of two types (related to atomic substitutions and atomic displacements) in films of a hyperstoichiometric cubic ($B1$ type) niobium nitride $NbN_{1.2}(C,O)$ with vacancies in the metallic sublattice. Niobium nitride films with an excessive content of nitrogen (compared to the stoichiometric composition $NbN_{1.0}$) were obtained by epitaxial deposition of niobium sputtered in an atmosphere of $Ar + xN_2$ ($0.15 < x < 0.7$) onto the (100) surface of a NaCl single crystal at the temperature 298–573 K [72, 73, 75]. The lattice parameter a_{B1} of the basic structure of the cubic niobium nitride $NbN_{1.2}(C,O)$ was equal to 0.439 nm; the size of coherent domains in the film was $\sim$ 30 nm.

In [72, 73], diffraction patterns of niobium nitride $NbN_{1.2}(C,O)$ corresponding to the (001), (112), (013), and (014) planes of the reciprocal lattice of the cubic phase were obtained; part of these patterns are shown in Fig. 11. The diffuse scattering distribution observed for niobium nitride differs from those revealed in the above-considered nonstoichiometric compounds (see Figs 6–10). It cannot be described using model clusters in the form of a tetrahedron, octahedron, or cubic unit cell of the fcc lattice; neither can it be described by combinations of these clusters. Indeed, a comparison of the experimental diffuse scattering contours (see Fig. 11) with the schemes of sections of the diffuse intensity surface (see Fig. 5) shows that they differ substantially.

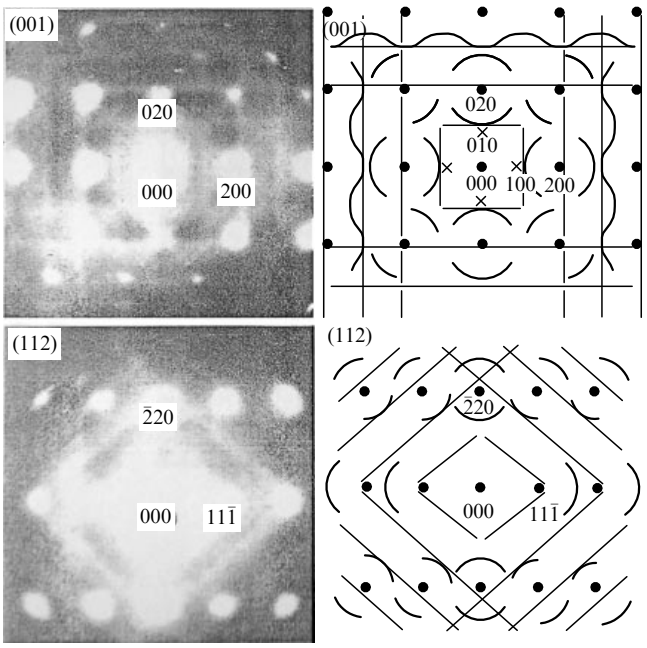

Figure 11. Diffuse scattering of electrons from a film of cubic niobium nitride $NbN_{1.2}(C,O)$ deposited at 573 K, and schemes of diffuse scattering distribution in the (001) and (112) planes of the reciprocal lattice [72, 73]. The reciprocal lattice points corresponding to fundamental (●) and forbidden (×) reflections are shown.

In the diffraction patterns of the hyperstoichiometric niobium nitride $NbN_{1.2}(C,O)$ [72, 73], intense diffuse scattering in the form of contacting flat and curvilinear regions is observed in addition to fundamental reflections of the cubic phase (see Fig. 11). The diffuse scattering regions do not pass through the reciprocal lattice points corresponding to fundamental reflections. The flat extended regions are parallel to the [100] and [010] directions of the reciprocal lattice and are displaced from the fundamental reflections of the cubic phase by the same vector $\Delta\mathbf{k}_{100}$ and $\Delta\mathbf{k}_{010}$, ($\Delta \cong 0.1$, $\mathbf{k}_{100} = [1\,0\,0]$ and $\mathbf{k}_{010} = [0\,1\,0]$ are the vectors of the reciprocal lattice of the cubic phase; $|\mathbf{k}_{100}| = |\mathbf{k}_{010}|$). The curved (having the form of arcs) diffuse scattering regions have a lower intensity than the flat regions. Their curvature radius is $\sim 0.9\,|\mathbf{k}_{100}|$ and the centers of the curvilinear regions are located at the points corresponding to fundamental reflections. It is obvious that these diffuse effects represent a set of sections of flat and spherical surfaces of the diffuse scattering intensity by the corresponding planes of the reciprocal lattice.

The existence of flat and spherical diffuse scattering regions was explained in [72–74] by the transition state of the niobium nitride related to the formation of a cubic or a tetragonal ordered phase in it, on the one hand, and by the existence of longitudinal waves of atomic displacements, on the other hand. As is seen from Fig. 11, the flat diffuse regions exist in the (001) section near both the fundamental [(200), (020)] and forbidden [(100), (010)] points of the reciprocal lattice of the cubic phase. The same is observed for other sections. If there is only a substitutional short-range order in the crystal, then the diffuse effects cannot occur near forbidden reflections [76]. The appearance of diffuse features near forbidden reflections is possible if substitutional waves correlated with displacement waves exist in the crystal. According to [73, 74], longitudinal waves of atomic displacements with wave vectors $\mathbf{K}_{100} \cong 0.1\mathbf{k}_{100}$ and $\mathbf{K}_{010} \cong 0.1\mathbf{k}_{010}$ and the corresponding waves of substitutions with wave vectors equal to $\sim 1.1\mathbf{k}_{100}$ and $\sim 1.1\mathbf{k}_{010}$ arise in the crystal lattice of niobium nitride $NbN_{1.2}(C,O)$. The spherical diffuse scattering regions are related to the longitudinal waves of atomic displacements whose wave vectors are $\sim 0.9\,|\mathbf{k}_{100}|$. Thus, the diffuse features that are observed in the hyperstoichiometric niobium nitride are due to the existence of short-range orders of two types, caused by substitutions and by displacements.

7. Diffuse scattering in titanium and vanadium monoxides

Among nonstoichiometric compounds, a special place belongs to cubic ($B1$ type) monoxides of titanium TiO_y ($0.80 \leqslant y \leqslant 1.25$) and vanadium VO_y ($0.85 \leqslant y \leqslant 1.23$), which have wide homogeneity regions. In the TiO_y and VO_y monoxides, structural vacancies exist simultaneously in two sublattices and the concentrations of vacancies in each sublattice can reach 15–17 at.%. The composition of these monoxides is written more accurately with the defects present in each sublattice taken into account as $TiO_y \equiv Ti_xO_z \equiv Ti_x\blacksquare_{1-x}O_z\square_{1-z}$, and $VO_y \equiv V_xO_z \equiv V_x\blacksquare_{1-x}O_z\square_{1-z}$, where $y = z/x$, and □ and ■ are the respective structural vacancies in the nonmetallic (oxygen) and metallic sublattices. Depending on the content of oxygen and conditions of heat treatment, the diffraction patterns of TiO_y and VO_y exhibit

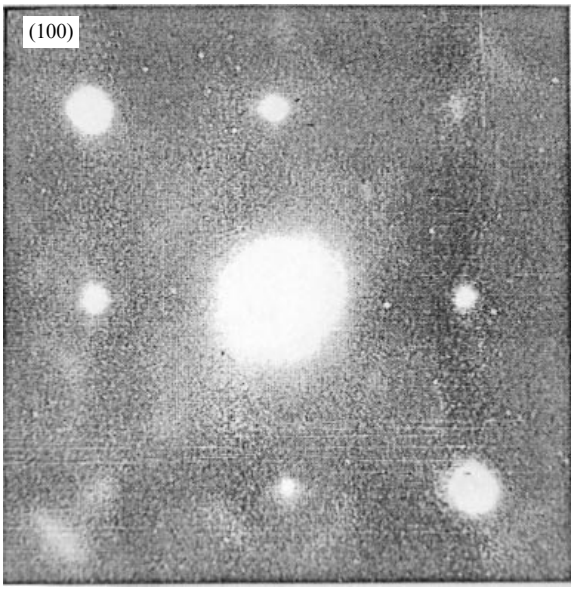

Figure 12. Diffraction pattern of cubic ($B1$ type) vanadium monoxide $VO_{0.95}$ [78]. The presence of weak diffuse maxima indicates a nonuniform distribution of structural vacancies, i.e., the existence of a short-range order [the (100) section of the reciprocal lattice is shown].

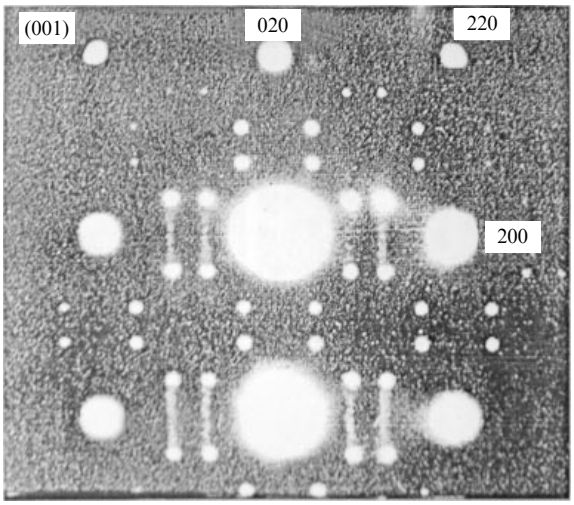

Figure 13. Diffraction pattern of ordered (space group $I4/m$) titanium monoxide $TiO_{1.25}$ (Ti_4O_5) [39, 77]. Along with fundamental and superlattice reflections, diffuse scattering maxima are seen, which indicate the presence of a short-range order in the sample [(001) section of the reciprocal lattice of the basic disordered cubic phase is shown].

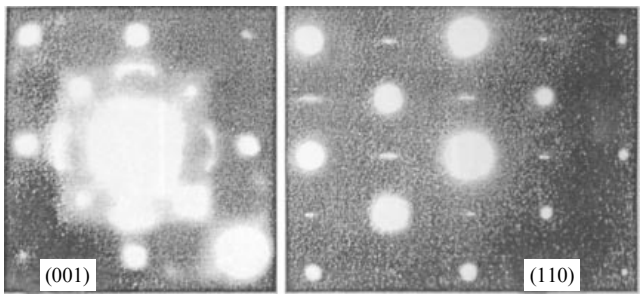

Figure 14. Diffuse scattering in the (001) and (110) sections of the reciprocal lattice of disordered cubic ($B1$ type) titanium monoxide $TiO_{1.00}$ [39].

diffuse effects [39, 40, 77–80] whose variety is due to the presence of two types of defects in these compounds and is related to the formation of transition states preceding the formation of ordered phases with different (cubic, tetragonal, orthorhombic, monoclinic) symmetries [1, 2].

Electron microscopy and electron diffraction were used in [78] to study samples of vanadium monoxides $VO_{1.25}$ and $VO_{0.95}$ preliminarily annealed for 30 h at 973 or 853 K. The annealing of $VO_{1.25}$ led to the appearance of clearly pronounced superlattice reflections in the diffraction pattern, which indicated the formation of the tetragonal ordered phase $V_{52}O_{64}$. The diffraction pattern of annealed $VO_{0.95}$ (Fig. 12) contained weak diffuse maxima along with fundamental reflections of the cubic phase. According to [78], the diffuse scattering arises due to a nonuniform distribution of structural vacancies in the lattice of the annealed $VO_{0.95}$, i.e., it is a consequence of a short-range order.

Electron diffraction was used in [39] to study short-range ordering of vacancies in a quenched cubic titanium monoxide TiO_y ($1.00 \leqslant y \leqslant 1.25$); experimental diffraction patterns for samples of $TiO_{1.00}$, $TiO_{1.19}$, and $TiO_{1.25}$ were obtained. In the case of quenching from 1473 K, some samples (e.g., $Ti_{1.00}$ and $TiO_{1.25}$) exhibited ordering, which follows from the presence of superlattice reflections (Fig. 13). The diffuse scattering observed indicates that the formation of the ordered phase has not been completed; the sample exhibits a substitutional short-range order. The samples of monoxide TiO_y without a long-range order were obtained by quenching from a higher temperature (1673 K). Diffuse scattering maxima were revealed in diffraction patterns obtained from disordered cubic monoxides $TiO_{1.00}$ (Fig. 14), $TiO_{1.19}$ (Fig. 15), and $TiO_{1.25}$. The location of the observed local maxima of diffuse scattering relative to the fundamental reflections differs strongly from that characteristic of the majority of cubic compounds such as $LiFeO_2$ [54], $LiNi_{0.4}Fe_{0.6}O_2$ [59], $Fe_{0.25}\square NbS_2$ [60], (Ti, Mo)C_x [61], or ZrN_y [66] (see Figs 6–10). In the diffraction patterns of the $TiO_{1.00}$ and $TiO_{1.19}$ monoxides, diffuse scattering maxima of two types exist in the (001) section, namely, pointlike in positions (110) and curved linear features extended in the [100] and [010] directions of the reciprocal lattice. In the (110) section, linear diffuse regions extended parallel to the [1 −1 0] direction are distinctly seen; however, it is clear from a comparison of analogous diffraction patterns for $TiO_{1.00}$, $TiO_{1.19}$, and $TiO_{1.25}$ that these linear diffuse features are degenerate spherical regions.

Ridder et al. [54], who analyzed the experimental results in [39], supposed that the observed set of diffuse features corresponds to diffuse scattering surfaces described by Eqns (47) and (48). In those places where the sections of these surfaces intersect one another, a local enhancement of intensity occurs, which looks like a pointlike maximum. This suggests that the diffuse scattering surface in nonstoichiometric monoxide TiO_y can be described in terms of the transition state model in which a cluster in the form of a cubic unit cell of the fcc lattice is taken into account along with an octahedron cluster.

The octahedral cluster and the cluster in the form of the cubic unit cell of the fcc lattice (a combination of the octahedral and simple cubic clusters) is used for simulating diffuse scattering related to the substitutional short-range

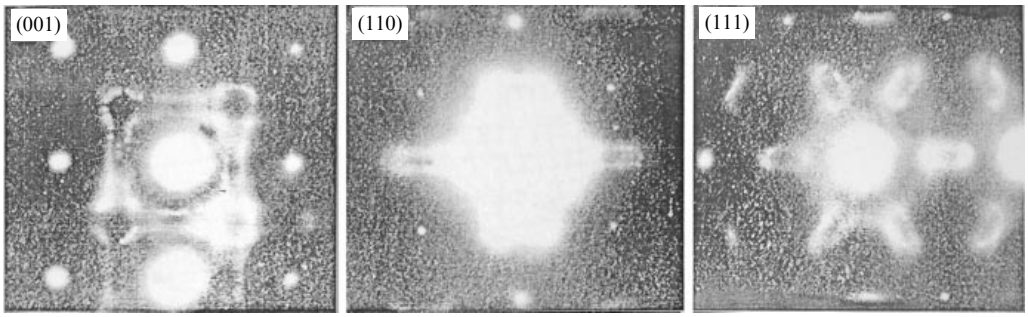

Figure 15. Electron-diffraction patterns from cubic ($B1$ type) titanium monoxide $TiO_{1.19}$ [39] in the (001), (110), and (111) sections of the reciprocal lattice. In the transition state model, the observed diffuse scattering was considered as a combination of the diffuse scattering surfaces described by Eqns (47) and (48).

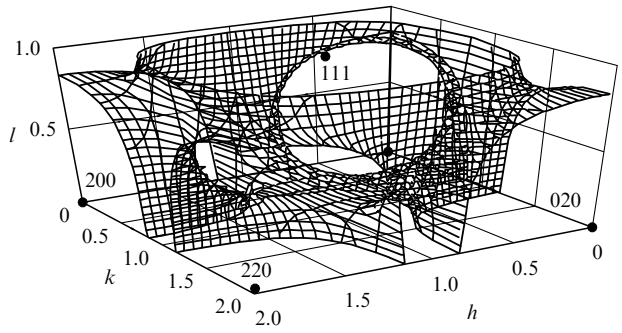

Figure 16. Distribution of diffuse scattering contours in the reciprocal lattice of an fcc crystal corresponding to model (47) with a tetrahedral cluster (schematic), and (●) the positions of the reciprocal lattice points (the part of the reciprocal lattice corresponding to $0 \leqslant h \leqslant 2$, $0 \leqslant k \leqslant 2$, and $0 \leqslant l \leqslant 1$ is shown).

order much more frequently than the tetrahedral cluster. The use of the tetrahedral cluster leads to the description of the diffuse scattering intensity surface by Eqn (47).

The three-dimensional distribution of the diffuse scattering intensity for the fcc lattice described by Eqn (47) at $C = 1$ is displayed in Fig. 16 (for simplicity, only a part of the reciprocal lattice with coordinates $0 \leqslant h \leqslant 2$, $0 \leqslant k \leqslant 2$, and $0 \leqslant l \leqslant 1$ is shown). It is seen that when using the tetrahedral cluster, the model diffuse scattering surface differs substantially from the surface in Fig. 4 corresponding to model (48) with a cluster in the form of a cubic unit cell (at $C > 0$) or with an octahedral cluster (at $C = 0$). In the first approximation, this surface can be represented (see Fig. 16) as a combined surface formed by the intersection of nine spherical surfaces (one sphere at the center and eight spheres in the vertices of the cube). Indeed, if we place spheres whose radii are somewhat smaller than half the lattice parameter into the sites of the unit cell of the bcc lattice, then the surface of the central sphere intersects the surfaces of the eight spheres located at the vertices of the unit cell.

We find the section of the diffuse scattering surface described by Eqn (47) with the (001) plane of the reciprocal lattice of the fcc crystal. For all sections by the planes of the (001) family, the value of l is an integer; therefore, $\cos \pi l \equiv 1$, and Eqn (47) becomes

$$\cos \pi h \cos \pi k + \cos \pi h + \cos \pi k + \left(1 - \frac{C}{4}\right) = 0\,, \qquad (63)$$

whence

$$k = \pm \frac{1}{\pi} \arccos\left(-1 + \frac{C}{4(1 + \cos \pi h)}\right) + 2m\,, \qquad (64)$$

where $m = 0, \pm 1, \pm 2, \ldots$. The sections of the diffuse scattering contours by the (001) plane of the reciprocal lattice calculated via Eqn (64) at $C = 1.0$ and $C = 0.81$ are shown in Fig. 17. As is seen, small changes in the parameter C have virtually no effect on the shape of the diffuse scattering contour.

The section of the diffuse scattering surface by the (110) plane is determined by the solution of Eqn (47) under the condition $h + k = 2n$, where $n = 0, \pm 1, \pm 2, \ldots$. In this case, $\cos \pi k \equiv \cos \pi h$; therefore, Eqn (47) becomes

$$\cos^2 \pi h + 2 \cos \pi h \cos \pi l + \left(1 - \frac{C}{4}\right) = 0\,,$$

which is solved by the function

$$l = \pm \frac{1}{\pi} \arccos\left(-\frac{\cos^2 \pi h + 1 - C/4}{2 \cos \pi h}\right) + 2m\,. \qquad (65)$$

Equation (47) obtained for a tetrahedral cluster has no analytic solutions for the sections of the diffuse scattering surface by arbitrary planes (hkl) with $h \neq 0$, $k \neq 0$, and $l \neq 0$. The sections of the diffuse scattering surface in (47) by the (111) and (112) planes of the reciprocal lattice that were obtained by numerical calculation at $C = 1.0$, and as the section by the (110) plane calculated by Eqn (65) at $C = 1.0$, are shown in Fig. 17.

We compare the experimental diffuse scattering in TiO_y [39] (see Figs 14, 15) with the contours (see Figs 5 and 17) calculated for model clusters in the form of a cubic unit cell and tetrahedron. It follows from the comparison that the experimental diffuse effects can indeed be described as a combination of the diffuse scattering surfaces corresponding to the two above-mentioned model clusters.

It was noted in [39] that the spatial distribution of diffuse scattering in titanium monoxide TiO_y resembles the Fermi surface of simple metals. To explain this similarity, the authors of [39] supposed that the titanium monoxide has high electron conductivity and, by analogy with metallic alloys, explained diffuse scattering by the occurrence of concentration waves or displacement waves in the crystal, whose wave vectors correspond to flat or cylindrical segments of the Fermi surface. However, the assumption about the high

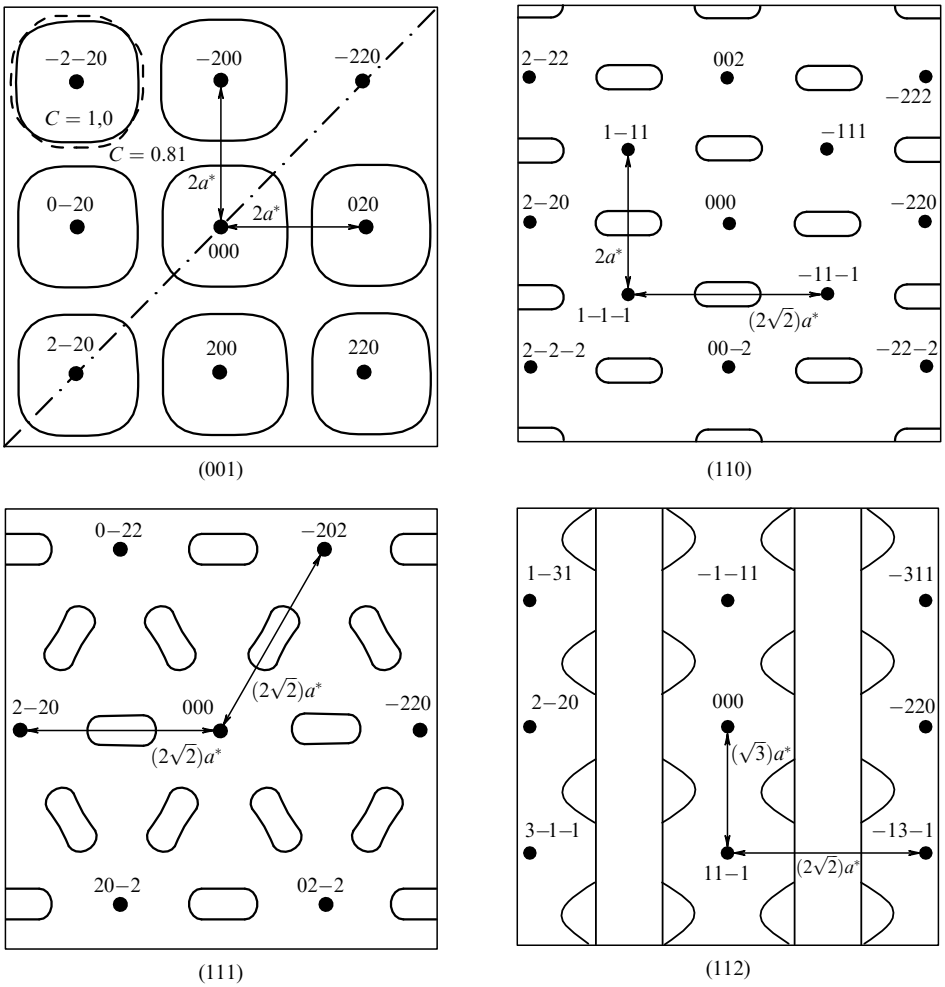

Figure 17. Sections of the diffuse scattering surface (described by Eqn (47) with the parameter $C = 1$) by the (001), (110), (111), and (112) planes of the reciprocal lattice of an fcc crystal. In the (001) section, a contour calculated for $C = 0.81$ is shown by a dashed line near the $(-2\ -2\ 0)$ site. Variations in the parameter C only weakly affect the shape of the diffuse scattering contour.

electron conductivity of TiO_y contradicts experiment; it follows from the spectra of bremsstrahlung, ultraviolet photoemission spectra [81], and data on optical conductivity [82] that there is a bandgap in the disordered TiO_y. The existence of a gap between the O2*p* and Ti3*d* bands of the electron energy spectrum of TiO_y follows from calculations in [83]. According to recent experimental results in [84–86], the disordered monoxides TiO_y with $y > 1.08$ are narrow-band semiconductors with the bandgap 0.17 eV and have low electron conductivity only at $y < 1.07$.

The authors of [79, 80] studied electron diffraction in annealed titanium monoxide $TiO_{1.087}$. The X-ray and electron diffraction results showed that the sample contained a monoclinic ordered phase of the Ti_5O_5 type. In the diffraction pattern of the ordered titanium monoxide, twin reflections and diffuse effects, as well as several weak reflections that could not be identified, have been revealed, along with fundamental and superlattice reflections. A direct confirmation of the existence of twins in the sample investigated was obtained by electron microscopy; in the micrograph of a sample of $TiO_{1.087}$, the authors of [79, 80, 87] revealed five twins in the form of extended rectangles. Figure 18 displays the electron diffraction pattern of the ordered monoclinic (space group $C2/m$) monoxide $TiO_{1.087}$, in which the diffuse effects are seen quite clearly, and a key diagram of this diffraction pattern. The normal to the figure plane, which is the matrix zone axis, corresponds to the $[011]^*_{C2/m} \equiv [112]^*_{B1}$ direction of the reciprocal lattice.

One feature of the diffraction pattern shown in Fig. 18 is the diffuse scattering in the form of a system of weak flat diffuse bands that are parallel to the [0 2 −1] and [2 0 −1] directions of the reciprocal lattice of the basic cubic phase and are slightly displaced with respect to the fundamental sites in the respective directions $\pm[-1\ 5\ -2]$ and $\pm[5\ -1\ -2]$. No single one of these bands passes through the (000) site. In the (112) section, the diffuse bands form a system of geometrically similar completely or partially closed rhombic contours concentrically located around the primary spot (000). If the contours passed through fundamental points (including forbidden reflections such as (−1 1 0), (1 −1 0), etc.), the ratio D/d of the lengths of the major and minor diagonals of any rhombus would be equal to $\sqrt{3}/\sqrt{2}$. Indeed, D_{id} is the distance between the sites $(n\,n-n$ and $-n-n\,n)$, where $n = 1, 2, 3, \ldots$, and therefore $D_{id} = = a^*\sqrt{3n}$, where a^* is the lattice parameter of the reciprocal lattice of the fcc crystal. Similarly, d_{id} is the distance between the sites $(-n\,n\,0)$ and $(n-n\,0)$, equal to $a^*\sqrt{2n}$. If shifts in the diffuse bands δ in the directions $\pm[1\ 0\ 0]$, $\pm[0\ 1\ 0]$, and $\pm[0\ 0\ 1]$ of the reciprocal lattice are equal to one another, then $D = (a^* + \delta)\sqrt{3n}$ and $d = (a^* + \delta)\sqrt{2n}$, and hence the ratio $D/d = (3/2)^{1/2}$ remains

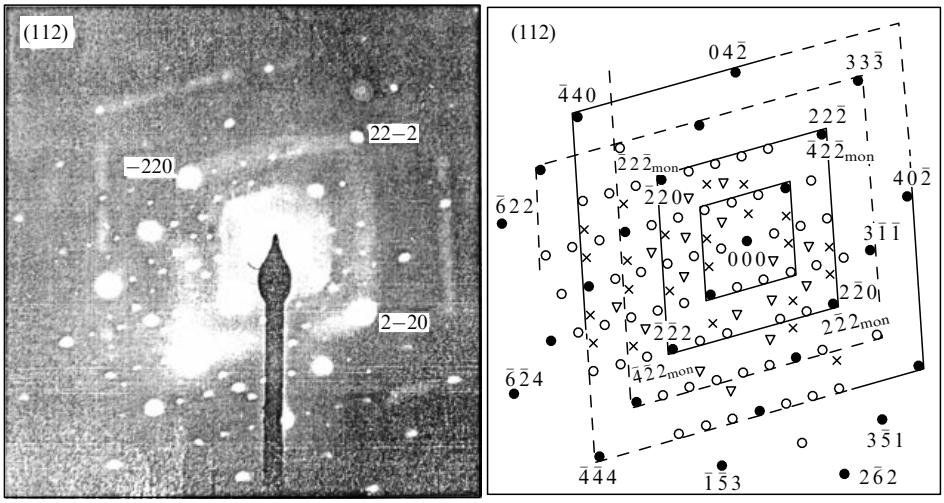

Figure 18. Experimental diffraction pattern of an ordered monoclinic (space group $C2/m$) titanium monoxide $TiO_{1.087}$ in the (112) section of the reciprocal lattice of the basic cubic phase and the related key pattern [80]: (●) fundamental reflections of the basic cubic ($B1$ type) structure of the disordered titanium monoxide; (○) superlattice reflections of the ordered monoclinic phase Ti_5O_5; (×) twin reflections of the ordered monoclinic phase Ti_5O_5; (▽) unidentified reflections (possibly reflections of an unknown ordered phase). The diffuse bands parallel to the [0 2 −1] and [2 0 −1] directions are shown by solid lines; weakly visible bands are shown by dashed lines. The matrix zone axis is $[112]^*_{B1} \equiv [011]^*_{C2/m}$. To facilitate comparison of the diffraction and key patterns, some fundamental and superlattice reflections are given in the diffraction pattern.

unaltered. If shifts occur only in the directions ±[0 0 1], then $D/d > (3/2)^{1/2}$ and the diagonals of the diffuse contour coincide with the directions [1 1 −1] and [1 −1 0]. If the bands are shifted only in the directions ±[1 0 0] and ±[0 1 0], we have $D/d < (3/2)^{1/2}$; if the shifts are equal in all directions, the minor diagonal coincides with the direction [1 −1 0]. If the diffuse bands are shifted only in the directions ±[1 0 0] or ±[0 1 0], the diagonals of the diffuse contour do not coincide with the directions [1 1 −1] and [1 −1 0], and $D/d \neq (3/2)^{1/2}$. In the diffraction pattern of titanium monoxide $TiO_{1.087}$, the ratio of the diagonals of the observed diffuse contours is $\sim (3/2)^{1/2}$ and the diagonals are parallel to the [1 1 −1] and [1 −1 0] directions. This means that in the three-dimensional reciprocal lattice, the diffuse contour that is nearest to the (000) site has the shape of a cube whose faces (walls) are diffuse planes shifted from this point by an equal distance $\delta_{100,010,001} = \Delta|\mathbf{k}_{100,010,001}|$ in the directions ±[1 0 0], ±[0 1 0], and ±[0 0 1] ($\mathbf{k}_{100} = [1\,0\,0]$, $\mathbf{k}_{010} = [0\,1\,0]$, $\mathbf{k}_{001} = [0\,0\,1]$, and $|\mathbf{k}_{100}| = |\mathbf{k}_{010}| = |\mathbf{k}_{001}|$). A numerical analysis of the diffraction pattern (Fig. 18) performed in [80] showed that the relative shift Δ is ∼ 0.07. Thus, the position of flat diffuse regions in reciprocal space can be specified by vectors

$$\mathbf{K}_{100} = \pm(\mathbf{k}_{h00} + \Delta\mathbf{k}_{100}) = \pm(h + \Delta)\,\mathbf{k}_{100}\,,$$
$$\mathbf{K}_{010} = \pm(\mathbf{k}_{0k0} + \Delta\mathbf{k}_{010}) = \pm(k + \Delta)\,\mathbf{k}_{010}\,,$$
$$\mathbf{K}_{001} = \pm(\mathbf{k}_{00l} + \Delta\mathbf{k}_{001}) = \pm(l + \Delta)\,\mathbf{k}_{001}\,,$$

which are normal to the corresponding diffuse planes.

According to [88], the periodic diffuse features that do not pass through the reciprocal-lattice points of the basic cubic phase can be related to the substitutional short-range order. However, the diffuse scattering observed in ordered titanium monoxide $TiO_{1.087}$ differs from the diffuse scattering characteristic of the majority of nonstoichiometric carbides and nitrides MX_y ($MX_y\square_{1-y}$) with the substitutional short-range order. It also differs from the diffuse scattering in disordered titanium monoxides $TiO_{1.00}$, $TiO_{1.19}$, and $TiO_{1.25}$ [39] (see Figs 14, 15). The only common feature is the existence of linear diffuse effects parallel to the [110] direction in the diffraction pattern of the (110) section of the reciprocal lattice of $TiO_{1.00}$. However, in the diffraction patterns presented in [39], these effects are local rather than extended; in addition, their linear character is rather a result of the degeneracy of spherical effects.

As noted above, the diffuse scattering in nonstoichiometric compounds MX_y with the basic structure of the $B1$ type in the case of a substitutional short-range order can be described in terms of an approximate cluster model of the transition state [52–55]. In this model, the diffuse scattering distribution in reciprocal space is described using a cubic, octahedral, or tetrahedral cluster (or their combination) in which all the sites (or part of its sites) are occupied by the X atoms. The spatial distribution of diffuse scattering in disordered TiO_y, which was found in [39], has also been successfully described in the transition state model using a combination of clusters in the form of a tetrahedron and a cubic unit cell.

However, the calculations performed showed that no single one of the above simple or combined model clusters allows obtaining diffuse scattering contours in the (112) section of the reciprocal lattice of an fcc crystal such as were observed in the diffraction pattern of ordered titanium monoxide $TiO_{1.087}$ in [79, 80]. Figures 19 and 20 display simulated contours of the (112) section of the diffuse scattering surfaces described by Eqns (48) or (47), respectively, in comparison with the experimental contours observed in the diffraction pattern of ordered monoclinic titanium monoxide $TiO_{1.087}$ [80]. It is clearly seen that the experimental diffuse scattering contours differ dramatically from the model contours corresponding to the substitutional short-range order. We note that the diffuse scattering caused by the substitutional short-range order is usually observed in samples of nonstoichiometric compounds quenched from a temperature that is somewhat greater than the order–disorder transition temperature. In other words, such diffuse scattering is characteristic of precisely a transition

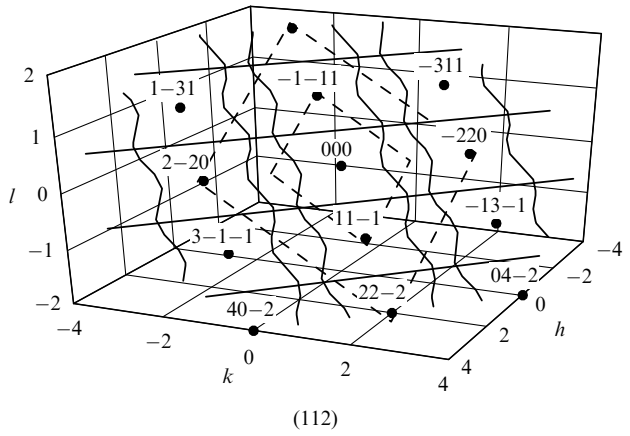

Figure 19. Diffuse scattering contours (schematic) and the positions of fundamental sites (●) in the (112) section of the reciprocal lattice of an fcc crystal. The substitutional short-range order was simulated using a cluster in the form of a unit cell of the fcc structure; correspondingly, the diffuse scattering surface is described by Eqn (48). The contours experimentally observed in the diffraction pattern of an ordered monoclinic (space group $C2/m$) titanium monoxide $TiO_{1.087}$ are shown by dashed lines; solid lines show model contours corresponding to the substitutional short-range order in the description of the diffuse scattering surface by Eqn (48) with the parameter $C = 3$.

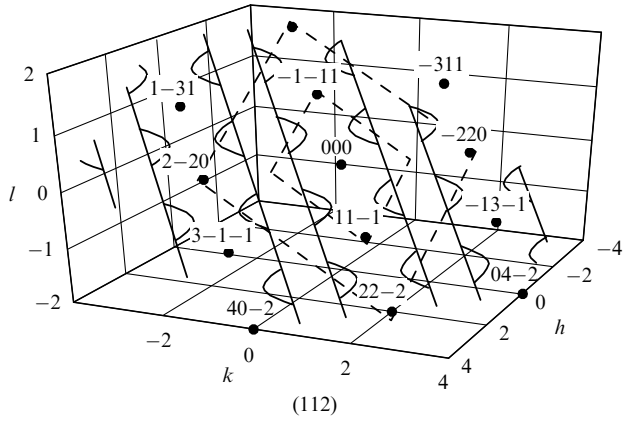

Figure 20. Diffuse scattering contours (schematic) and the positions of fundamental nodes (●) in the (112) section of the reciprocal lattice of an fcc crystal. The substitutional short-range order was simulated using a tetrahedral cluster. The contours experimentally observed in the diffraction pattern of an ordered monoclinic (space group $C2/m$) titanium monoxide $TiO_{1.087}$ are shown by dashed lines; solid lines correspond to model contours corresponding to the substitutional short-range order in the description of the diffuse scattering surface by Eqn (47) with the parameter $C = 1$.

state [52 – 55]. In [79, 80], the diffraction pattern was obtained from an ordered nonstoichiometric titanium monoxide; therefore, no diffuse scattering due to the substitutional short-range order is present in it. According to the theory of diffraction from imperfect crystals in [76], flat regions of diffuse scattering can be caused by atomic displacement waves. With this in mind, the authors of [80] supposed that atomic-displacement waves occur in ordered titanium monoxide $TiO_{1.087}$ that involve restricted flat regions of reciprocal space with the fixed values of wave vectors $\mathbf{K}_{100} \cong \pm(h + 0.07)\,\mathbf{k}_{100}$, $\mathbf{K}_{010} \cong \pm(k + 0.07)\,\mathbf{k}_{010}$, and $\mathbf{K}_{001} \cong \pm(l + 0.07)\,\mathbf{k}_{001}$. It is near these vectors that the maxima of diffuse scattering intensity caused by the short-range order related to displacements are located. Thus, the results in [80] suggest that upon formation of a monoclinic superstructure Ti_5O_5 in the nonstoichiometric cubic titanium monoxide $TiO_{1.087}$, not only does a redistribution of atoms and structural vacancies occurs but also atomicdisplacement waves arise.

Similar diffuse scattering bands were observed in [72 – 74] in the diffraction patterns of epitaxially deposited films of the nonstoichiometric cubic niobium nitride $NbN_{1.2}(C,O)$ with vacancies in the niobium sublattice (Fig. 11). The presence of vacancies in the metallic sublattice unites the titanium monoxide $TiO_{1.087}$ and the niobium nitride $NbN_{1.2}(C,O)$ and distinguishes them from other nonstoichiometric compounds with structural vacancies present only in the nonmetallic sublattice. Nevertheless, the difference in the diffraction patterns of titanium monoxide [80] and niobium nitride [72, 73] is sufficiently large. In the diffraction pattern of ordered titanium monoxide, no diffuse scattering characteristic of the substitutional short-range order is present and the intensity of flat diffuse scattering contours caused by atomic displacements is much weaker than in the diffraction pattern of the niobium nitride.

8. Conclusions

The most characteristic feature of strongly nonstoichiometric compounds is the high concentration of structural vacancies, which can vary from zero to several dozen percent at the lower boundary of the homogeneity region. The large concentration of vacancies is a prerequisite for the existence of a disorder or an order in the distribution of atoms and vacancies in the structure of nonstoichiometric compounds. Deviations from the statistical (disordered) distribution of atoms and vacancies manifest themselves in the appearance of a short-range order or a long-range order in the crystal structure of nonstoichiometric compounds.

Experimental investigations of nonstoichiometric compounds (carbides, nitrides, oxides, ternary oxides of alkali metals such as lithium ferrite) and solid solutions of these compounds performed using diffraction methods revealed various effects of diffuse scattering. The appearance of maxima of diffuse scattering in diffraction patterns is due to the formation of a substitutional short-range order or a short-range order related to atomic displacements or both. Thus, the investigation of diffuse scattering allows clarifying fine details of the crystal structure of nonstoichiometric compounds. The short-range order and correlations in compounds and solid solutions with substitutable metallic atoms of various sorts can be most conveniently studied using diffuse scattering of X-rays. In compounds where a redistribution of nonmetallic atoms of various sorts or metallic atoms and structural vacancies can occur, the most informative methods are neutron and electron scattering. For studying complex disordered systems, the most convenient method is diffraction electron microscopy, because the realization of an image (in real space) in a single experiment and of a diffraction pattern (in reciprocal space) is an obvious advantage in structural investigations.

In the case of a substitutional short-range order, the topology of the diffuse scattering intensity in reciprocal space can be described in terms of a sufficiently simple structural model of a transition state [52 – 55]. The transition state directly precedes the formation of the long-range order and is simulated using one or a few clusters whose structure

corresponds to the geometry of the crystal lattice of the compound under consideration.

Extended flat regions of diffuse scattering that do not pass through the reciprocal lattice points corresponding to fundamental reflections and are observed in diffraction patterns of ordered phases of nonstoichiometric compounds are due to the appearance of waves of atomic displacements. The atomic displacement waves involve restricted flat regions of reciprocal space with fixed values of wave vectors.

The experimental results on diffuse scattering in strongly nonstoichiometric compounds described in the literature show that the substitutional short-range order is retained at temperatures that can be higher by 300 – 400 K than the temperature of the reversible equilibrium order – disorder transition. This means that short-range order should necessarily be taken into account in an analysis of the structure and theoretical description of phase transformations in nonstoichiometric compounds.

Acknowledgments. This work was supported in part by the Russian Foundation for Basic Research, project no. 06-03-32047a.

References

1. Gusev A I, Rempel' A A *Nestekhiometriya, Besporyadok i Poryadok v Tverdom Tele* (Nonstoichiometry, Disorder, and Order in Solids)
2. Gusev A I, Rempel A A, Magerl A J *Disorder and Order in Strongly Nonstoichiometric Compounds*: *Transition Metal Carbides, Nitrides, and Oxides* (Berlin: Springer, 2001)
3. Gusev A I, Rempel' A A *Strukturnye Fazovye Perekhody v Nestekhiometricheskikh Soedineniyakh* (Structural Phase Transitions in Nonstoichiometric Compounds) (Moscow: Nauka, 1988)
4. Gusev A I *Fizicheskaya Khimiya Nestekhiometricheskikh Tugoplavkikh Soedinenii* (Physical Chemistry of Nonstoichiometric Refractory Compounds) (Moscow: Nauka, 1991)
5. Rempel' A A *Effekty Uporyadocheniya v Nestekhiometricheskikh Soedineniyakh Vnedreniya* (Effects of Ordering in Nonstoichiometric Interstitial Compounds) (Ekaterinburg: Nauka, 1992)
6. Gusev A I *Usp. Khim.* **57** 1595 (1989) [*Russ. Chem. Rev.* **57** 913 (1988)]
7. Gusev A I *Phys. Status Solidi B* **156** 11 (1989)
8. Nazarova S Z, Gusev A I *Zh. Strukt. Khim.* **42** 563 (2001) [*J. Struct. Chem.* **42** 470 (2001)]
9. Gusev A I, Nazarova S Z *Usp. Fiz. Nauk* **175** 681 (2005) [*Phys. Usp.* **48** 651 (2005)]
10. Krivoglaz M A, Smirnov A A *Teoriya Uporyadochivayushchikhsya Splavov* (Theory of Ordering Aloys) (Moscow: Fizmatgiz, 1958)
11. Smirnov A A *Theoriya Splavov Vnedreniya* (Theory of Interstitial Aloys) (Moscow: Nauka, 1979)
12. Khachaturyan A G *Teoriya Fazovykh Prevrashchenii i Struktura Tverdykh Rastvorov* (Theory of Phase Transformations and the Structure of Solid Solutions) (Moscow: Nauka, 1974)
13. Bethe H A *Proc. R. Soc. London Ser. A* **150** 552 (1935)
14. Cowley J M *Phys. Rev.* **77** 669 (1950)
15. Warren B E, Averbach B L, Roberts B W *J. Appl. Phys.* **22** 1493 (1951)
16. Krivoglaz M A *Teoriya Rasseyaniya Rentgenovskikh Luchei i Teplovykh Neitronov Real'nymi Kristallami* (Theory of X-ray and Thermal-Neutron Scattering by Real Crystals) (Moscow: Nauka, 1967) [Translated into English (New York: Plenum Press, 1969)]
17. Iveronova V I, Katsnel'son A A *Blizhnii Poryadok v Tverdykh Rastvorakh* (Short-Range Order in Solid Solutions) (Moscow: Nauka, 1977)
18. Gusev A I, Rempel A A *Phys. Status Solidi A* **84** 527 (1984)
19. Moisy-Maurice V et al. *Solid State Commun.* **39** 661 (1981)
20. Priem T "Etude de l'ordre a courte distance dans les carbures et nitrures non-stoechiometriques de metaux de transition par diffusion diffuse de neutrons", Rapport CEA-R-5499 (Gif-sur-Yvette: Commissariat a l'Energie Atomique, Centre d'Etudes Nucleaires de Saclay, 1989)
21. Sparks C J, Borie B, in *Local Atomic Arrangements Studied by X-ray Diffraction*: *Proc. of a Symp., Chicago, Ill., 1965* (Metallurgical Soc. Conf., Vol. 36, Eds J B Cohen, J E Hilliard) (New York: Gordon and Breach, 1966) p. 5
22. Beuneu B et al. *J. Appl. Crystallogr.* **23** 497 (1990)
23. Sauvage M, Parthé E *Acta Crystallogr. A* **28** 607 (1972)
24. Sauvage M, Parthé E, Yelon W B *Acta Crystallogr. A* **30** 597 (1974)
25. Billingham J, Bell P S, Lewis M H *Acta Crystallogr. A* **28** 602 (1972)
26. De Novion C H, Maurice V *J. Phys. Colloq.* (Paris) **38** C7-211 (1977)
27. Fender B E F, in *Chemical Applications of Thermal Neutron Scattering* (Eds B T M Willis) (London: Oxford Univ. Press, 1973) p. 250
28. Priem T et al. *Solid State Commun.* **63** 929 (1987)
29. Priem T et al. *Physica B* **156 – 157** 47 (1989)
30. Priem T et al. *J. Phys* (Paris) **50** 2217 (1989)
31. Priem T, Beuneu B, de Novion C H, in *X-ray and Neutron Structure Analysis in Materials Science* (Ed. J Hašek) (New York: Plenum Press, 1989) p. 149
32. De Novion C H et al., in *The Physics and Chemistry of Carbides, Nitrides, and Borides* (NATO ASI Series. Ser. E, No. 185, Ed. R Freer) (Dordrecht: Kluwer Acad. Publ., 1990) p. 329
33. Moisy-Maurice V "Structure atomique des carbures non-stoechiometriques de metaux de transition", Rapport CEA-R-5127 (Gif-sur-Yvette: Commissariat a l'Energie Atomique, Centre d'Etudes Nucleaires de Saclay, 1981)
34. Christensen A N *J. Cryst. Growth* **33** 99 (1976)
35. Buršík J, Weatherly G C *Phys. Status Solidi A* **174** 327 (1999)
36. Rempel' A A, Gusev A I *Fiz. Tverd. Tela* **32** 16 (1990) [*Sov. Phys. Solid. State* **32** 8 (1990)]
37. Rempel A A, Gusev A I *Phys. Status Solidi B* **160** 389 (1990)
38. Hiraga K, Hirabayashi M *J. Phys. Colloq.* (Paris) **38** C7-224 (1977)
39. Castles J R, Cowley J M, Spargo A E C *Acta Crystallogr. A* **27** 376 (1971)
40. Terauchi H, Cohen J B *Acta Crystallogr. A* **35** 646 (1979)
41. Umanskii Ya S, Fadeeva V I *Fiz. Met. Metalloved.* **19** 473 (1965)
42. Umanskii Ya S, Fadeeva V I *Fiz. Met. Metalloved.* **20** 719 (1965)
43. Umanskii Ya S, Fadeeva V I *Izv. Akad. Nauk SSSR, Neorg. Mater.* **2** 82 (1966)
44. Umanskii Ya S, Fadeeva V I *Kristallografiya* **11** 130 (1966)
45. Umanskii Ya S, Myuller A S *Izv. Vyssh. Uchebn. Zaved., Chern. Metall.* (7) 130 (1969)
46. Umanskii Ya S, Myuller A S *Izv. Vyssh. Uchebn. Zaved., Chern. Metall.* (1) 128 (1970)
47. Rudman P S *Acta Metall.* **12** 1381 (1964)
48. Gorbacheva T B et al. *Fiz. Met. Metalloved.* **39** 768 (1975)
49. Katsnel'son A A, Gorbacheva T B *Fiz. Met. Metalloved.* **32** 742 (1971)
50. Katsnel'son A A, Gorbacheva T B, Rybal'chenko R B *Fiz. Met. Metalloved.* **34** 211 (1972)
51. Clapp P C, Moss S C *Phys. Rev.* **171** 754 (1968)
52. De Ridder R, van Tendeloo G, Amelinckx S *Acta Crystallogr. A* **32** 216 (1976)
53. De Ridder R et al. *Phys. Status Solidi A* **38** 663 (1976)
54. De Ridder R et al. *Phys. Status Solidi A* **40** 669 (1977)
55. De Ridder R, in *Diffraction and Imaging Techniques in Material Science* 2nd ed. (Eds S Amelinckx, R Gevers, J Van Landuyt) (Amsterdam: North-Holland Publ. Co., 1978) p. 429
56. Brunel M, de Bergevin F *J. Phys. Chem. Solids* **30** 2011 (1969)
57. Buršík J, Weatherly G C *Phys. Status Solidi A* **176** 835 (1999)
58. Sommerfeld A, Bethe H A, in *Handbuch der Physik* Vol. 24, 2nd ed. (Berlin: Springer, 1933) p. 333
59. Kellerman D G, Shalaeva E V, Gusev A I *Fiz. Tverd. Tela* **46** 1633 (2004) [*Phys. Solid State* **46** 1686 (2004)]
60. Van Tendeloo G, Amelinckx S, in *The Chemistry of Extended Defects in Non-Metallic Solids*: *Proc. of the Inst. for Advanced Study, Scottsdale, Arizona, USA, 1969* (Eds L Eyring, M O'Keeffe) (Amsterdam: North-Holland Publ. Co., 1970) p. 97
61. Murata Y, Yukawa N *J. Less-Common Met.* **141** 235 (1988)
62. Murata Y et al. *J. Less-Common Met.* **141** 309 (1988)
63. Ohshima K et al. *Acta Crystallogr. A* **44** 167 (1988)

64. Chevalier J-P A A, Stobbs W M *Acta Metall.* **24** 535 (1976)
65. Venables J D, Lye R G *Philos. Mag.* **19** 565 (1969)
66. Li P, Howe J M *Acta Mater.* **51** 1261 (2003)
67. Seitz F, Koehler J S, in *Solid State Physics. Advances in Research and Applications* Vol. 2 (Eds F Seitz, D Turnbull) (New York: Academic Press, 1956) p. 305
68. Morillo J, de Novion C H, Dural J *Radiat. Eff.* **55** 67 (1981)
69. Allison C Y, Stoller R E, Kenik E A *J. Appl. Phys.* **63** 1740 (1988)
70. Gosset D et al. *Radiat. Eff. Defects Solids* **118** 207 (1991)
71. Morillo J, Le T N, Jackierowicz G *Ann. Chim.* (France) **16** 397 (1991)
72. Shalaeva E V et al. *J. Phys. IV Colloq.* (Paris) **1** C2-209 (1991)
73. Shalaeva E V, Mitrofanov B V, Shveikin G P *Phys. Status Solidi A* **154** 505 (1996)
74. Shalaeva E V, Borisov S V, Makhnev A A, in *Khimiya Tverdogo Tela. Struktura, Svoistva i Primenenie Novykh Neorganicheskikh Materialov* (Chemistry of Solids: Structure, Properties, and Application of New Inorganic Materials) (Eds G P Shveikin, A L Ivanovskii) (Ekaterinburg: Inst. Khimii Tverdogo Tela UrO RAN, 1998) p. 56
75. Shalaeva E V et al. *Thin Solid Films* **261** 64 (1995)
76. Guinier A *X-ray Diffraction in Crystals, Imperfect Crystals, and Amorphous Bodies* (New York: Dover, 1994)
77. Watanabe D et al., in *The Chemistry of Extended Defects in Non-Metallic Solids*: *Proc. of the Inst. for Advanced Study, Scattsdale, Arizona, USA, 1969* (Eds L Eyring, M O'Keeffe) (Amsterdam: North-Holland Publ. Co., 1970) p. 238
78. Bell P S, Lewis M H *Phys. Status Solidi A* **7** 431 (1971)
79. Valeeva A A et al. *Pis'ma Zh. Eksp. Teor. Fiz.* **77** 28 (2003) [*JETP Lett.* **77** 25 (2003)]
80. Valeeva A A, Gusev A I *Pis'ma Zh. Eksp. Teor. Fiz.* **79** 579 (2004) [*JETP Lett.* **79** 468 (2004)]
81. Barman S R, Sarma D D *Phys. Rev. B* **49** 16141 (1994)
82. Gokhale S, Barman S R, Sarma D D *Phys. Rev. B* **52** 14526 (1995)
83. Leung C et al. *Phys. Rev. B* **54** 7857 (1996)
84. Valeeva A A, Rempel' A A, Gusev A I *Pis'ma Zh. Eksp. Teor. Fiz.* **73** 702 (2001) [*JETP Lett.* **73** 621 (2001)]
85. Valeeva A A, Rempel' A A, Gusev A I *Dokl. Ross. Akad. Nauk* **382** 320 (2002) [*Dokl. Phys.* **47** 39 (2002)]
86. Gusev A I, Valeeva A A *Fiz. Tverd. Tela* **45** 1185 (2003) [*Phys. Solid State* **45** 1242 (2003)]
87. Valeeva A A et al *Fiz. Tverd. Tela* **45** 84 (2003) [*Phys. Solid State* **45** 87 (2003)]
88. Cowley J M *Diffraction Physics* 3rd ed. (Amsterdam: Elsevier, 1995)